

# Discrete FEM-BEM coupling with the Generalized Optimized Schwarz Method

Antonin Boisneault<sup>[0000-0001-7986-9048]</sup> \*<sup>1,2</sup>, Marcella Bonazzoli<sup>[0000-0002-0284-5643]</sup><sup>2</sup>,  
 Xavier Claeys<sup>[0000-0003-0826-6244]</sup><sup>1</sup>, and Pierre Marchand<sup>[0000-0002-2522-6837]</sup><sup>1</sup>

<sup>1</sup>POEMS, CNRS, Inria, ENSTA, Institut Polytechnique de Paris, 91120 Palaiseau, France

<sup>2</sup>Inria, Unité de Mathématiques Appliquées, ENSTA, Institut Polytechnique de Paris, 91120 Palaiseau, France

## Abstract

The present contribution aims at developing a non-overlapping Domain Decomposition (DD) approach to the solution of acoustic wave propagation boundary value problems based on the Helmholtz equation, on both bounded and unbounded domains. This DD solver, called Generalized Optimized Schwarz Method (GOSM), is a substructuring method, that is, the unknowns of an iteration are associated with the subdomains interfaces. We extend the analysis presented in [20] to a fully discrete setting. We do not consider only a specific set of boundary conditions, but a whole class including, e.g., Dirichlet, Neumann, and Robin conditions. Our analysis will also cover interface conditions corresponding to a Finite Element Method - Boundary Element Method (FEM-BEM) coupling. In particular, we shall focus on three classical FEM-BEM couplings, namely the Costabel, Johnson-Nédélec and Bielak-MacCamy couplings. As a remarkable outcome, the present contribution yields well-posed substructured formulations of these classical FEM-BEM couplings for wavenumbers different from classical spurious resonances. We also establish an explicit relation between the dimensions of the kernels of the initial variational formulation, the local problems and the substructured formulation. That relation especially holds for any wavenumber for the substructured formulation of Costabel FEM-BEM coupling, which allows us to prove that the latter formulation is well-posed even at spurious resonances. Besides, we introduce a systematically geometrically convergent iterative method for the Costabel FEM-BEM coupling, with estimates on the convergence speed.

**Acknowledgements:** This work is funded by the Inria program “Actions exploratoires” (OptiGPR3D)  
**Mathematics Subject Classification:** 65R20 · 65N22 · 65N38 · 35J05 · 65N55

## Introduction

In this work, our aim is to design an efficient solver for acoustic wave propagation modelled by the Helmholtz equation. The objective is to develop a numerical method that is versatile enough to accommodate heterogeneous and complex environments, while remaining efficient and tailored to high performance computing. Two classes of methods are often used for the numerical simulation of time-harmonic wave propagation: the finite element method (FEM),

---

\*Corresponding author: antonin.boisneault@inria.fr

which is versatile and suited to heterogeneous materials, and the boundary element method (BEM), which performs best on piecewise homogeneous materials and/or unbounded domains. In order to optimally handle different types of materials, we seek a numerical algorithm to systematically couple and benefit from these two methods.

To this end, we introduce a new FEM-BEM coupling strategy based on a substructuring domain decomposition method called *Generalized Optimized Schwarz Method* (GOSM). Substructuring DD methods involve

- a non-overlapping partition of the domain of interest,
- resolution of local problems with optimized boundary conditions in each subdomain that can be performed in parallel,
- an iterative resolution of a substructured problem, that is, a problem on the skeleton (the union of the boundaries of the subdomains).

The novelty of our approach lies in the extension to FEM-BEM coupling of recent developments from [23, 20]. One of the strengths of this current work is a clear well-posedness and convergence theory.

Research on domain decomposition methods for time-harmonic wave propagation started with a proper choice of transmission condition at the interface between subdomains. In [32], a first convergent DD method was introduced for the Helmholtz equation using impedance transmission conditions, where the impedance coefficient is  $\imath\kappa$  and  $\kappa$  the wavenumber. To accelerate the possibly slow convergence, several approaches have been explored to replace the impedance coefficient by a local transmission operator, see e.g. [35, 13].

Another approach studied in [24] is to replace the impedance coefficient with a non-local impedance operator, which ensures provable geometric convergence. A strong requirement for such a fast convergence is the absence of cross-points, i.e. points shared by more than two subdomains in the domain partition. All the previous methods are usually called Optimized Schwarz Methods (OSM). To treat cross-points, [23, 20] recently introduced the GOSM, which uses a non-local impedance operator, and also a non-local exchange operator  $\Pi$  instead of the usual swap operator between subdomains, used in the OSMs.

Classical FEM-BEM couplings, such as the Costabel [28], Johnson-Nédélec [40], and Bielak-MacCamy [8] couplings, rely on Dirichlet and Neumann transmission conditions between the FEM and BEM subdomains. Meanwhile, new FEM-BEM couplings have been developed building on the progress of DD methods for the Helmholtz equation. For example, the Després impedance condition has been used in [7], while [17, 18] employ local transmission operators as in [13]. All the previous works consider a partition into two subdomains, one bounded FEM subdomain and one unbounded BEM subdomain. With more than two subdomains, the additional challenge related to cross-points has not been often studied in the literature. In [14], one additional unknown per cross-point is considered, which results in solving, per iteration, one additional (sparse) linear system in each FEM subdomain, and finally a dense linear system (whose size equals the number of cross-points). Citing [14], “the local problems remain coupled at the cross-points”. In [12], a proper functional framework dealing with cross-points has been designed, and new multidomain FEM-BEM formulations have been proposed and analyzed in a continuous setting, but their practical implementation is not straightforward.

We propose here a discrete counterpart of the analysis presented in [20] and extend it to FEM-BEM coupling. Note that in [20], only bounded domains are considered, and physical

conditions on their boundary are weakly imposed via additional boundary unknowns. The classical FEM-BEM couplings are reformulated as (35), that is, a substructured equation of the form  $\text{Id} + \Pi S$  where

- $\Pi$  is the non-local exchange operator mentioned above,
- $S$  is a scattering operator, which takes ingoing impedance traces, solves the local problems and returns the outgoing impedance traces.

We prove that the substructured reformulations are well-posed<sup>1</sup>, when the classical FEM-BEM couplings are. Besides, when the considered FEM-BEM coupling satisfies a sign assumption related to physical dissipation (see Equation (16)),  $\Pi S$  is a contraction<sup>2</sup> (see Lemma 5.3 and Proposition 6.7). Thus, the substructured system can be solved using a Richardson solver with guaranteed geometric convergence (see Theorem 10.1), even when cross-points are present. The sign assumption (16) is satisfied by the Costabel coupling (Proposition 3.4), but not by the Johnson-Nédélec and Bielak-MacCamy couplings (Proposition 3.5), for which a GMRes [50] iterative solver can be used instead (when these couplings are well-posed).

Additionally, when the sign assumption (16) is satisfied, an explicit relation is established between the dimension of the kernels of the classical variational formulation, the local problems, and the substructured formulation (see Theorem 7.3). Note that classical FEM-BEM couplings can have a non-trivial kernel even when the initial boundary value problem is well-posed, a phenomenon commonly referred to as *spurious resonances*, see e.g. [53].

Finally, we explain the implementation details of the GOSM, and illustrate its properties with thorough numerical experiments. Remark that subdomains can be associated either with volume unknowns for FEM subdomains, or with boundary unknowns for BEM subdomains and physical boundary conditions. Thus, we discuss the choice of the impedance operators, and we observe that convergence is improved by picking them according to the nature of the subdomains (FEM vs BEM vs boundary condition). Moreover, we show that  $h$ -robust geometric convergence can be achieved even with cross-points.

The article is structured as follows. After introducing notations in Section 1 and the considered boundary value problems in Section 2, we recall the classical FEM-BEM couplings and discuss the validity of the sign assumption (16) for their formulations. Section 4 presents the discretization framework used throughout the paper, while Section 5 introduces the domain decomposition building blocks, such as the impedance and exchange operators. The GOSM formulation is derived in Section 6 based on the scattering operator  $S$ , and its well-posedness is treated in Section 7. A relation between the inf-sup constants of the initial variational problem and its substructured reformulation is given in Section 8. Section 9 is about the extension to more general settings, and Section 10 presents the numerical investigation.

## 1 Notation conventions

To proceed further into the description and the analysis of the boundary value problem and the domain decomposition method we wish to study, we need now to fix a few notational conventions. The present section is mainly here for reference, as most of the conventions we adopt are classical. All vector spaces that we are going to consider have  $\mathbb{C}$  as a scalar field.

---

<sup>1</sup>Well-posedness is intended in the classical Hadamard sense (and not in the weaker Fredholm sense).

<sup>2</sup>The terms *contractive* and *contraction* are employed here as in [16]: the inequality is not necessarily strict.

**Dual spaces** Assuming that  $H$  is a Banach space equipped with the norm  $\|\cdot\|_H$ , its topological dual, denoted  $H^*$ , will systematically be equipped with the norm

$$\|\varphi\|_{H^*} := \sup_{v \in H \setminus \{0\}} \frac{|\varphi(v)|}{\|v\|_H}.$$

The canonical duality pairing will be denoted  $\langle \cdot, \cdot \rangle: H^* \times H \rightarrow \mathbb{C}$  and defined by  $\langle \varphi, v \rangle := \varphi(v)$ . Although the space  $H$  does not appear explicitly in the notation “ $\langle \varphi, v \rangle$ ”, when such pairing angle brackets are used, it shall be clear from the context which pair of spaces  $(H, H^*)$  is under consideration. We emphasize that the duality pairings we consider do *not* involve any complex conjugation. We shall write  $\langle v, \varphi \rangle = \langle \varphi, v \rangle$ ,  $\forall v \in H, \varphi \in H^*$  indifferently.

**Inf-sup constants and adjoints** Assuming that  $V$  is another Banach space equipped with the norm  $\|\cdot\|_V$ , and  $L: H \rightarrow V$  is a bounded linear map, we shall refer to its *inf-sup constant* denoted and defined as follows

$$\text{infsup}(L) := \inf_{H \rightarrow V} \frac{\|L(u)\|_V}{\|u\|_H}. \quad (1)$$

In the case where  $L$  is invertible, this inf-sup constant equals the inverse of the continuity modulus of  $L^{-1}$ . The inf-sup constant is well-defined even if  $L$  is not invertible though. The *adjoint*<sup>3</sup> of the map  $L: H \rightarrow V$  shall be defined as the unique bounded linear map  $L^*: V^* \rightarrow H^*$  satisfying

$$\langle L^*(p), u \rangle := \langle p, L(u) \rangle \quad (2)$$

for all  $p \in V^*$  and all  $u \in H$ . When  $V = H$ , the map  $L$  is said *symmetric* if  $L^* = L$ . Once again, we insist that no complex conjugation comes into play in (2). The bounded linear map  $L$  induces another bounded linear map  $\bar{L}: H \rightarrow V$  defined by  $\bar{L}(\bar{u}) := \overline{L(u)}$  for all  $u \in H$ .

**Annihilator** For any subset  $X \subset H$ , we denote its *annihilator* (or *polar set*) by

$$X^\circ := \{\varphi \in H^* \mid \langle \varphi, v \rangle = 0, \forall v \in X\}, \quad (3)$$

see, e.g. [49, §4.6], [16, §1.3] and [9, §4.1.4–4.1.5]. We point out three important properties. First, using [16, Theorem 2.16], let  $Y$  and  $Z$  be two closed subspaces in  $H$ . If  $Z + Y$  is closed in  $H$ , then

$$Z^\circ + Y^\circ = (Z \cap Y)^\circ. \quad (4)$$

By applying Definition (3) to  $\text{Im}(L) \subset V$ , note that for *any* bounded linear map  $L: H \rightarrow V$ ,

$$\text{Im}(L)^\circ = \text{Ker}(L^*). \quad (5)$$

Finally, if  $L: H \rightarrow V$  is a bounded linear map with *closed range*, then

$$\text{Im}(L) = \text{Ker}(L^*)^\circ. \quad (6)$$

---

<sup>3</sup>This adjoint operator, which does not involve complex conjugation, is sometimes referred to as *quasi-adjoint*, see e.g. [19]. We follow here the notational convention of [16, §2.6] and [49, §4.10].

**Scalar products** A bounded linear operator  $T: H \rightarrow H^*$  is called *self-adjoint* if  $\overline{T} = T^*$  and, in this case we have  $\langle T(u), \overline{u} \rangle \in \mathbb{R}$  for all  $u \in H$ . It is called *positive definite* if  $\langle T(u), \overline{u} \rangle \in (0, +\infty)$  for all  $u \in H \setminus \{0\}$ . If  $T$  is both self-adjoint and positive definite, the sesquilinear form  $u, v \mapsto \langle T(u), \overline{v} \rangle$  induces a scalar product over  $H$  and the associated norm is denoted

$$\|u\|_T := \sqrt{\langle T(u), \overline{u} \rangle}.$$

**Cartesian products** We shall also consider Cartesian products  $H_1 \times \cdots \times H_J$  where each  $H_j$  is a Banach space equipped with the norm  $\|\cdot\|_{H_j}$ . Then the Cartesian product shall be equipped with the following canonical norm and duality pairings

$$\begin{aligned} \|\mathbf{v}\|_{H_1 \times \cdots \times H_J}^2 &:= \|v_1\|_{H_1}^2 + \cdots + \|v_J\|_{H_J}^2 \\ \langle \mathbf{v}, \mathbf{q} \rangle &:= \langle v_1, q_1 \rangle + \cdots + \langle v_J, q_J \rangle \end{aligned}$$

for  $\mathbf{v} = (v_1, \dots, v_J), v_j \in H_j$ , and  $\mathbf{q} = (q_1, \dots, q_J), q_j \in H_j^*$ . If  $V_j, j = 1, \dots, J$ , is another collection of Banach spaces and  $L_j: H_j \rightarrow V_j$  are bounded linear maps, we shall also consider the block-diagonal operator  $\text{diag}(L_1, \dots, L_J)$ , mapping  $H_1 \times \cdots \times H_J$  onto  $V_1 \times \cdots \times V_J$  and defined, for  $\mathbf{v} = (v_1, \dots, v_J), v_j \in H_j$ , and  $\mathbf{q} = (q_1, \dots, q_J), q_j \in V_j^*$ , by

$$\langle \mathbf{q}, \text{diag}(L_1, \dots, L_J) \mathbf{v} \rangle := \langle q_1, L_1(v_1) \rangle + \cdots + \langle q_J, L_J(v_J) \rangle.$$

**Pseudo-inverses** Finally, we shall also need to refer to the Moore-Penrose pseudo-inverse (or generalized inverse). We recall briefly its definition, and refer our reader to e.g. [6, 43, 48] for more details. Assume that  $(H, \|\cdot\|_H)$  and  $(V, \|\cdot\|_V)$  are two Hilbert spaces and  $L: H \rightarrow V$  is a bounded linear map with closed range. By definition, its *Moore-Penrose pseudo-inverse* is the unique bounded linear operator  $L^\dagger: V \rightarrow H$  satisfying the four conditions

- (i)  $L \cdot L^\dagger \cdot L = L$
- (ii)  $L^\dagger \cdot L \cdot L^\dagger = L^\dagger$
- (iii)  $L^\dagger \cdot L: H \rightarrow H$  is an orthogonal projector
- (iv)  $L \cdot L^\dagger: V \rightarrow V$  is an orthogonal projector

(7)

The properties above imply in particular that

$$\text{Im}(L \cdot L^\dagger) = \text{Im}(L), \tag{8a}$$

$$\text{Ker}(L^\dagger \cdot L) = \text{Ker}(L). \tag{8b}$$

In the case where  $L: H \rightarrow V$  is bounded and surjective, its pseudo-inverse is characterized by

$$L \cdot L^\dagger = \text{Id} \quad \text{and} \quad \|L^\dagger(u)\|_H = \min\{\|v\|_H, L(v) = u\}. \tag{9}$$

Similarly, in the case where  $L: H \rightarrow V$  is bounded and one-to-one, the pseudo-inverse is characterized as a left inverse  $L^\dagger \cdot L = \text{Id}$  satisfying the optimality property  $\|u - L \cdot L^\dagger(u)\|_V = \min\{\|u - L(v)\|_V, v \in H\}$ .

## 2 Problems under consideration

In dimension  $d = 2$  or  $3$ , let  $\Omega \subset \mathbb{R}^d$  be a polyhedral bounded open set, and denote  $\Gamma := \partial\Omega$  its boundary. We shall consider the space of square integrable measurable functions  $L^2(\Omega) := \{v: \Omega \rightarrow \mathbb{C}, \|v\|_{L^2(\Omega)}^2 := \int_{\Omega} |v(\mathbf{x})|^2 d\mathbf{x} < +\infty\}$ , and the Sobolev space  $H^1(\Omega) := \{v \in L^2(\Omega), \nabla v \in L^2(\Omega)\}$  equipped with  $\|v\|_{H^1(\Omega)}^2 := \|\nabla v\|_{L^2(\Omega)}^2 + \tilde{k}^2 \|v\|_{L^2(\Omega)}^2$ , where  $\tilde{k} > 0$  is some fixed parameter. We shall also consider  $H_0^1(\Omega)$ , which is the closure of  $\mathcal{C}_{0,c}^\infty(\Omega) := \{\varphi|_\Omega, \varphi \in \mathcal{C}^\infty(\mathbb{R}^d), \text{with bounded support } \text{supp}(\varphi) \subset \Omega\}$  for  $\|\cdot\|_{H^1(\Omega)}$ , and the space  $H_{\text{loc}}^1(\mathbb{R}^d) := \{v, \varphi v \in H^1(\mathbb{R}^d) \forall \varphi \in \mathcal{C}_c^\infty(\mathbb{R}^d)\}$ , where  $\mathcal{C}_c^\infty(\mathbb{R}^d)$  is the set of compactly supported  $\mathcal{C}^\infty$  functions. Lastly, we consider a source term  $f \in L^2(\mathbb{R}^d)$  supported in  $\Omega$ , and a measurable function  $\kappa: \mathbb{R}^d \rightarrow \mathbb{C}$  modelling a wavenumber and satisfying

**Assumption:** (10)

$$\Im\{\kappa(\mathbf{x})^2\} \geq 0 \quad \forall \mathbf{x} \in \Omega,$$

as well as  $\kappa(\mathbf{x}) = \tilde{k} > 0$  for  $\mathbf{x} \in \mathbb{R}^d \setminus \Omega$ , and  $\sup \text{ess}_{\mathbb{R}^d} |\kappa| < +\infty$ . We wish to develop a solution strategy for boundary value problems modelling acoustic wave propagation and taking one of the following generic forms

$$\begin{aligned} u \in H^1(\Omega) \quad &\text{and} \quad -\Delta u - \kappa^2 u = f \quad \text{in } \Omega \\ &+ \text{boundary condition on } \Gamma = \partial\Omega, \end{aligned} \quad (11a)$$

$$\begin{aligned} u \in H_{\text{loc}}^1(\mathbb{R}^d) \quad &\text{and} \quad -\Delta u - \kappa^2 u = f \quad \text{in } \mathbb{R}^d \\ &+ \text{Sommerfeld's radiation condition.} \end{aligned} \quad (11b)$$

Note that in (11b)  $\Gamma = \partial\Omega$  is seen as a fictitious interface on which are imposed Dirichlet and Neumann transmission conditions. Sommerfeld's radiation condition at infinity can be expressed as (see, e.g. [44, §2.6.5])

**Sommerfeld's condition:** (12)

$$\lim_{r \rightarrow \infty} \int_{\partial\mathcal{B}_r} |\partial_r u - \imath k u|^2 ds = 0$$

where  $\mathcal{B}_r$  is the ball centered at 0 with radius  $r$ ,  $\partial_r$  denotes the radial derivative, and  $ds$  refers to the Lebesgue surface measure on  $\partial\mathcal{B}_r$ .

Let us examine how to write a variational formulation of Problems (11). Taking the cue from [20] to deal with boundary value problems of the form (11a), we first introduce  $\mathcal{A}_\Omega: H^1(\Omega) \rightarrow H^1(\Omega)^*$  and  $\ell_\Omega \in H^1(\Omega)^*$  that, for all  $u, v \in H^1(\Omega)$ , are defined by

$$\begin{aligned} \langle \mathcal{A}_\Omega(u), v \rangle &:= \int_{\Omega} (\nabla u \cdot \nabla v - \kappa^2 u v) d\mathbf{x}, \\ \langle \ell_\Omega, v \rangle &:= \int_{\Omega} f v d\mathbf{x}. \end{aligned} \quad (13)$$

To *weakly* impose the boundary condition of (11a), first we consider the trace space  $H^{1/2}(\Gamma) := \{v|_\Gamma, v \in H^1(\Omega)\}$ , equipped with the norm  $\|v|_\Gamma\|_{H^{1/2}(\Gamma)} := \inf_{v_0 \in H_0^1(\Omega)} \|v + v_0\|_{H^1(\Omega)}$ . Its dual

shall be denoted  $H^{-1/2}(\Gamma) := H^{1/2}(\Gamma)^*$ , with  $\|p\|_{H^{-1/2}(\Gamma)} := \sup_{v \in H^{1/2}(\Gamma) \setminus \{0\}} |\langle p, v \rangle| / \|v\|_{H^{1/2}(\Gamma)}$ . Then we introduce a bounded operator

$$\mathcal{A}_\Gamma: H^{+1/2}(\Gamma) \times H^{-1/2}(\Gamma) \rightarrow H^{-1/2}(\Gamma) \times H^{+1/2}(\Gamma)$$

whose precise definition depends on the boundary/interface condition we wish to take into account in (11). Several boundary conditions for (11a) have been discussed in [20]. For example a Dirichlet boundary condition can be weakly imposed by choosing (see [20, Example 3.1])

$$\text{Dirichlet:} \quad \mathcal{A}_\Gamma = \begin{bmatrix} 0 & \text{Id} \\ \text{Id} & 0 \end{bmatrix}. \quad (14)$$

A Neumann boundary condition can be weakly imposed by taking (see [20, Example 3.2])

$$\text{Neumann:} \quad \mathcal{A}_\Gamma = \begin{bmatrix} 0 & 0 \\ 0 & \mathcal{T}_\Gamma^{-1} \end{bmatrix}, \quad (15)$$

where  $\mathcal{T}_\Gamma: H^{1/2}(\Gamma) \rightarrow H^{-1/2}(\Gamma)$  is the bounded linear map defined by  $\langle \mathcal{T}_\Gamma(v), \bar{v} \rangle := \|v\|_{H^{1/2}(\Gamma)}^2$ ,  $\forall v \in H^{1/2}(\Gamma)$ . Due to (10),  $\Im\{\langle \mathcal{A}_\Omega(v), \bar{v} \rangle\} \leq 0$ ,  $\forall v \in H^1(\Omega)$  and, as shown in [20], a similar property holds for the boundary operators  $\mathcal{A}_\Gamma$  in (14) and (15), and for those associated with other classical boundary conditions (Robin, mixed Dirichlet-Neumann). We state this property as an assumption that shall be further discussed in the subsequent analysis

**Assumption:**

$$\begin{aligned} \Im\{\langle \mathcal{A}_\Gamma(v, q), (\bar{v}, \bar{q}) \rangle\} &\leq 0 \\ \forall v \in H^{+1/2}(\Gamma), \quad \forall q \in H^{-1/2}(\Gamma). \end{aligned} \quad (16)$$

As discussed in [20], once the operator  $\mathcal{A}_\Gamma$  has been defined in accordance with the boundary condition to be imposed, the boundary value problem (11a) can be reformulated into the following variational form

$$\begin{aligned} \text{Find } u \in H^1(\Omega), \quad p \in H^{-1/2}(\Gamma) \text{ such that} \\ \langle \mathcal{A}_\Omega(u), v \rangle + \langle \mathcal{A}_\Gamma(u|_\Gamma, p), (v|_\Gamma, q) \rangle &= \langle \ell_\Omega, v \rangle + \langle \ell_\Gamma, (v|_\Gamma, q) \rangle \\ \forall v \in H^1(\Omega), \quad \forall q \in H^{-1/2}(\Gamma), \end{aligned} \quad (17)$$

where  $\ell_\Omega \in H^1(\Omega)^*$  and  $\ell_\Gamma \in H^{-1/2}(\Gamma) \times H^{+1/2}(\Gamma)$  are known source terms related to the function  $f$  and the right-hand side of the boundary condition in Problem (11a).

We are going to develop a discrete counterpart of the theory proposed in [20]. Choosing  $\mathcal{A}_\Gamma$  as (14) or (15) for (11a), two situations can occur: either (11a), and thus (17), is well-posed<sup>1</sup>, or it is not. The latter can happen for a cavity problem when  $\kappa$  is a resonance. In both cases, (17) will be rewritten as a substructured form after decomposing the domain  $\Omega$ .

In the next section we exhibit other choices of  $\mathcal{A}_\Gamma$  to reformulate also Problem (11b) into the generic form (17). This can be achieved by means of FEM-BEM coupling schemes, which model the Dirichlet and Neumann transmission conditions on  $\Gamma = \partial\Omega$ , the Helmholtz equation with constant wavenumber in  $\mathbb{R}^d \setminus \Omega$ , and Sommerfeld's radiation condition at infinity.

### 3 FEM-BEM coupling

We are particularly interested in FEM-BEM coupling and one of the goal of the present contribution is to design a numerical strategy that systematically converges, with proven convergence bounds, toward the solution to a FEM-BEM formulation. In the present section, we introduce a few notations related to layer potentials and boundary integral operators, in order to then define  $\mathcal{A}_\Gamma$  for FEM-BEM coupling formulations.

Denote  $\mathbf{x} \mapsto \mathcal{G}_k(\mathbf{x})$  the outgoing *Green kernel* for the Helmholtz operator with constant wavenumber  $k > 0$ . For  $d = 3$ , this is  $\mathcal{G}_k(\mathbf{x}) := \exp(ik|\mathbf{x}|)/(4\pi|\mathbf{x}|)$  and, for  $d = 2$ , this is  $\mathcal{G}_k(\mathbf{x}) := iH_0^{(1)}(k|\mathbf{x}|)/(4\pi)$ , where  $z \mapsto H_0^{(1)}(z)$  is the 0-th order Hankel function of the first kind, see e.g. [45, Chap.10]. For any sufficiently smooth pair of Dirichlet and Neumann traces  $(v, p)$ , we define the *total layer potential operator* by the formula

$$\begin{aligned} \mathcal{G}_\Gamma(v, p)(\mathbf{x}) := & \int_\Gamma (\mathbf{n}(\mathbf{y}) \cdot (\nabla \mathcal{G}_k)(\mathbf{x} - \mathbf{y})) v(\mathbf{y}) \\ & + \mathcal{G}_k(\mathbf{x} - \mathbf{y}) p(\mathbf{y}) \, ds(\mathbf{y}), \quad \mathbf{x} \in \mathbb{R}^d \setminus \Gamma, \end{aligned} \quad (18)$$

where  $ds$  refers to the Lebesgue surface measure on  $\Gamma$  and  $\mathbf{n}: \Gamma \rightarrow \mathbb{R}^d$  is the unit vector field normal to  $\Gamma$  directed toward the exterior of  $\Omega$ . The map  $(v, p) \mapsto \mathcal{G}_\Gamma(v, p)|_\Omega$  can be extended by density as a bounded linear operator  $H^{1/2}(\Gamma) \times H^{-1/2}(\Gamma) \rightarrow H^1(\Delta, \bar{\Omega}) := \{v \in H^1(\Omega), \Delta v \in L^2(\Omega)\}$ , see e.g. [51, Thm.3.1.16] or [42, Thm.6.11]. Similarly,  $(v, p) \mapsto \mathcal{G}_\Gamma(v, p)|_{\mathbb{R}^d \setminus \Omega}$  can be extended by density as a bounded linear operator  $H^{1/2}(\Gamma) \times H^{-1/2}(\Gamma) \rightarrow H^1_{loc}(\Delta, \mathbb{R}^d \setminus \Omega)$ .

We stress that, because of the convolutional form of the potential operator (18) and the properties of the outgoing Green kernel, for any pair  $(v, p) \in H^{1/2}(\Gamma) \times H^{-1/2}(\Gamma)$ , the function  $u(\mathbf{x}) := \mathcal{G}_\Gamma(v, p)(\mathbf{x})$  satisfies Sommerfeld's condition at infinity (12), see [54, 55, 58, 44], as well as the Helmholtz equation with wavenumber  $k > 0$  in  $\mathbb{R}^d \setminus \Omega$ , see e.g. [27, §2.4].

Next, we define the *Dirichlet-Neumann interior trace map*  $\gamma_\Gamma: H^1(\Delta, \bar{\Omega}) \rightarrow H^{1/2}(\Gamma) \times H^{-1/2}(\Gamma)$  as the unique bounded linear operator satisfying, for all  $\varphi \in \mathcal{C}^\infty(\bar{\Omega}) := \{\varphi|_\Omega, \varphi \in \mathcal{C}^\infty(\mathbb{R}^d)\}$ , the formula

$$\gamma_\Gamma(\varphi) := (\varphi|_\Gamma, \mathbf{n} \cdot \nabla \varphi|_\Gamma).$$

We emphasize that traces are taken from the interior of  $\Omega$  here. Similarly, we define the *Dirichlet-Neumann exterior trace map*  $\gamma_{\Gamma,c}: H^1_{loc}(\Delta, \mathbb{R}^d \setminus \Omega) \rightarrow H^{1/2}(\Gamma) \times H^{-1/2}(\Gamma)$  as the unique bounded linear map satisfying  $\gamma_{\Gamma,c}(\varphi) := (\varphi|_\Gamma, \mathbf{n} \cdot \nabla \varphi|_\Gamma)$  for all  $\varphi \in \mathcal{C}^\infty(\mathbb{R}^d \setminus \Omega)$  where, this time, traces are taken from the exterior of  $\Omega$  (with  $\mathbf{n}$  still directed toward the exterior of  $\Omega$ ).

With Dirichlet-Neumann trace maps, we can form  $\frac{1}{2}(\gamma_\Gamma + \gamma_{\Gamma,c}) \cdot \mathcal{G}_\Gamma: H^{1/2}(\Gamma) \times H^{-1/2}(\Gamma) \rightarrow H^{1/2}(\Gamma) \times H^{-1/2}(\Gamma)$ , which is commonly decomposed into a  $2 \times 2$  matrix of *boundary integral operators*

$$\frac{1}{2}(\gamma_\Gamma + \gamma_{\Gamma,c}) \cdot \mathcal{G}_\Gamma = \begin{bmatrix} \mathcal{K}_\Gamma & \mathcal{V}_\Gamma \\ \mathcal{W}_\Gamma & \tilde{\mathcal{K}}_\Gamma \end{bmatrix} \quad (19)$$

where the bounded operators  $\mathcal{V}_\Gamma: H^{-1/2}(\Gamma) \rightarrow H^{+1/2}(\Gamma)$  (*single-layer operator*),  $\mathcal{W}_\Gamma: H^{+1/2}(\Gamma) \rightarrow H^{-1/2}(\Gamma)$  (*hypersingular operator*),  $\mathcal{K}_\Gamma: H^{+1/2}(\Gamma) \rightarrow H^{+1/2}(\Gamma)$  (*double layer operator*), and  $\tilde{\mathcal{K}}_\Gamma: H^{-1/2}(\Gamma) \rightarrow H^{-1/2}(\Gamma)$  (*adjoint double layer operator*) can simply be defined so as to comply with (19). Both single-layer and hypersingular operators are symmetric, while  $\mathcal{K}_\Gamma^* = -\tilde{\mathcal{K}}_\Gamma$ .

FEM-BEM coupling can be achieved by certain choices of  $\mathcal{A}_\Gamma$  involving the operators in (19). These choices model the Dirichlet and Neumann transmission conditions on  $\Gamma$ , the Helmholtz equation with wavenumber  $k > 0$  in  $\mathbb{R}^d \setminus \Omega$ , and Sommerfeld's condition (12). Several FEM-BEM couplings exist, and here we shall concentrate on three of them, which were reviewed in e.g. [4].

**Example 3.1** (Symmetric Costabel coupling [28, 29]). *It is classically written as two equations: find  $u \in H^1(\Omega)$ ,  $p \in H^{-1/2}(\Gamma)$  such that*

$$\begin{aligned} \langle \mathcal{A}_\Omega(u), v \rangle + \int_\Gamma \mathcal{W}_\Gamma(u|_\Gamma) v|_\Gamma \, ds + \int_\Gamma (\text{Id}/2 + \tilde{\mathcal{K}}_\Gamma)(p) v|_\Gamma \, ds &= \langle \ell_\Omega, v \rangle \\ \int_\Gamma (\text{Id}/2 - \mathcal{K}_\Gamma)(u|_\Gamma) q \, ds - \int_\Gamma \mathcal{V}_\Gamma(p) q \, ds &= 0 \end{aligned}$$

$\forall v \in H^1(\Omega)$ ,  $\forall q \in H^{-1/2}(\Gamma)$ , with  $\mathcal{A}_\Omega$  and  $\ell_\Omega$  defined in (13). After summing the two equations, it fits formulation (17) by taking  $\ell_\Gamma = 0$  and

$$\text{Costabel: } \mathcal{A}_\Gamma = \begin{bmatrix} \mathcal{W}_\Gamma & \text{Id}/2 + \tilde{\mathcal{K}}_\Gamma \\ \text{Id}/2 - \mathcal{K}_\Gamma & -\mathcal{V}_\Gamma \end{bmatrix}. \quad (20)$$

Note that  $\mathcal{A}_\Gamma^* = \mathcal{A}_\Gamma$ , hence the name symmetric for the Costabel coupling.

**Example 3.2** (Johnson-Nédélec coupling [40, 52, 56]). *It is classically written as two equations: find  $u \in H^1(\Omega)$ ,  $p \in H^{-1/2}(\Gamma)$  such that*

$$\begin{aligned} \langle \mathcal{A}_\Omega(u), v \rangle + \int_\Gamma p v|_\Gamma \, ds &= \langle \ell_\Omega, v \rangle \\ \int_\Gamma (\text{Id}/2 - \mathcal{K}_\Gamma)(u|_\Gamma) q \, ds - \int_\Gamma \mathcal{V}_\Gamma(p) q \, ds &= 0 \end{aligned}$$

$\forall v \in H^1(\Omega)$ ,  $\forall q \in H^{-1/2}(\Gamma)$ , with  $\mathcal{A}_\Omega$  and  $\ell_\Omega$  defined in (13). After summing the two equations, it fits formulation (17) by taking  $\ell_\Gamma = 0$  and

$$\text{Johnson-Nédélec: } \mathcal{A}_\Gamma = \begin{bmatrix} 0 & \text{Id} \\ \text{Id}/2 - \mathcal{K}_\Gamma & -\mathcal{V}_\Gamma \end{bmatrix}. \quad (21)$$

**Example 3.3** (Bielak-MacCamy coupling [8]). *It is classically written as two equations: find  $u \in H^1(\Omega)$ ,  $p \in H^{-1/2}(\Gamma)$  such that*

$$\begin{aligned} \langle \mathcal{A}_\Omega(u), v \rangle + \int_\Gamma (\text{Id}/2 + \tilde{\mathcal{K}}_\Gamma)(p) v|_\Gamma \, ds &= \langle \ell_\Omega, v \rangle \\ \int_\Gamma u|_\Gamma q \, ds - \int_\Gamma \mathcal{V}_\Gamma(p) q \, ds &= 0 \end{aligned}$$

$\forall v \in H^1(\Omega)$ ,  $\forall q \in H^{-1/2}(\Gamma)$ , with  $\mathcal{A}_\Omega$  and  $\ell_\Omega$  defined in (13). After summing the two equations, it fits formulation (17) by taking  $\ell_\Gamma = 0$  and

$$\text{Bielak-MacCamy: } \mathcal{A}_\Gamma = \begin{bmatrix} 0 & \text{Id}/2 + \tilde{\mathcal{K}}_\Gamma \\ \text{Id} & -\mathcal{V}_\Gamma \end{bmatrix}. \quad (22)$$

It is natural to ask whether the FEM-BEM couplings above comply with the imaginary part sign assumption (16). As a matter of fact, only the Costabel coupling fits this hypothesis.

**Proposition 3.4.**

*Operator (20) for the Costabel coupling fulfills Assumption (16).*

*Proof.* For the sake of brevity, set  $[(u, p), (v, q)]_\Gamma := \langle u, q \rangle - \langle v, p \rangle$  and  $\mathfrak{A}_\Gamma := \frac{1}{2}(\gamma_\Gamma + \gamma_{\Gamma,c}) \cdot \mathcal{G}_\Gamma$ , see (19). Then, with  $\mathcal{A}_\Gamma$  defined by (20), observe that  $\langle \mathcal{A}_\Gamma(u, p), (v, q) \rangle = -[\mathfrak{A}_\Gamma(u, p), (v, q)]_\Gamma + (\langle u, q \rangle + \langle v, p \rangle)/2$ . This implies  $\Im\{\langle \mathcal{A}_\Gamma(u, p), (\bar{u}, \bar{p}) \rangle\} = -\Im\{[\mathfrak{A}_\Gamma(u, p), (\bar{u}, \bar{p})]_\Gamma\}$  because  $\langle u, \bar{p} \rangle + \langle \bar{u}, p \rangle = \langle u, \bar{p} \rangle + \overline{\langle u, \bar{p} \rangle} = 2\Re\{\langle u, \bar{p} \rangle\}$ . Finally, according to [12, Proposition A.2] or [44, Lemma 3.2.1],  $\Im\{[\mathfrak{A}_\Gamma(u, p), (\bar{u}, \bar{p})]_\Gamma\} \geq 0$  for all  $(u, p) \in H^{1/2}(\Gamma) \times H^{-1/2}(\Gamma)$ . This concludes the proof.  $\square$

**Proposition 3.5.**

*Operators (21) and (22) for the Johnson-Nédélec and Bielak-MacCamy couplings do not fulfill Assumption (16).*

*Proof.* We construct a pair  $(\Phi, P) \in H^{1/2}(\Gamma) \times H^{-1/2}(\Gamma)$  such that  $\Im\{\langle \mathcal{A}_\Gamma(\Phi, P), (\bar{\Phi}, \bar{P}) \rangle\} > 0$  in the case of the Johnson-Nédélec coupling. A similar construction can be made for the Bielak-MacCamy coupling. For all  $\phi \in H^{1/2}(\Gamma)$ ,  $p \in H^{-1/2}(\Gamma)$

$$\begin{aligned} \langle \mathcal{A}_\Gamma(\phi, p), (\bar{\phi}, \bar{p}) \rangle &= \langle p, \bar{\phi} \rangle + \langle (\text{Id}/2 - \mathcal{K}_\Gamma)\phi - \mathcal{V}_\Gamma p, \bar{p} \rangle \\ &= \langle p, \bar{\phi} \rangle + \langle \phi, \bar{p} \rangle - \langle (\text{Id}/2 + \mathcal{K}_\Gamma)\phi, \bar{p} \rangle - \langle \mathcal{V}_\Gamma p, \bar{p} \rangle \\ &= \langle p, \bar{\phi} \rangle + \overline{\langle \phi, \bar{p} \rangle} - \langle (\text{Id}/2 + \mathcal{K}_\Gamma)\phi, \bar{p} \rangle - \langle \mathcal{V}_\Gamma p, \bar{p} \rangle \\ &= 2\Re\{\langle p, \bar{\phi} \rangle\} - \langle (\text{Id}/2 + \mathcal{K}_\Gamma)\phi, \bar{p} \rangle - \langle \mathcal{V}_\Gamma p, \bar{p} \rangle. \end{aligned}$$

According to [34, Lemma 3.1],  $\Im\{\langle \mathcal{V}_\Gamma p, \bar{p} \rangle\} \geq 0$ . Our goal is then to find a pair  $(\phi, p)$  such that  $-\Im\{(\text{Id}/2 + \mathcal{K}_\Gamma)\phi, \bar{p}\} > \Im\{\langle \mathcal{V}_\Gamma p, \bar{p} \rangle\}$ . Consider any invertible real positive definite operator  $T: H^{1/2}(\Gamma) \rightarrow H^{-1/2}(\Gamma)$ . According to the Fredholm alternative,  $\dim \text{Ker}(\text{Id}/2 + \mathcal{K}_\Gamma) < +\infty$ , so  $\text{Ker}(\text{Id}/2 + \mathcal{K}_\Gamma) \neq H^{1/2}(\Gamma)$  and there exists  $\phi \in H^{1/2}(\Gamma)$  satisfying  $\|(\text{Id}/2 + \mathcal{K}_\Gamma)\phi\|_T > 0$ . Let  $\alpha > 0$  be some real parameter whose value will be chosen appropriately below, and set  $p_\alpha := \alpha p$  with  $p := \iota T(\text{Id}/2 + \mathcal{K}_\Gamma)\phi$ . We obtain

$$\langle \mathcal{A}_\Gamma(\phi, p_\alpha), (\bar{\phi}, \bar{p}_\alpha) \rangle = 2\Re\{\langle p_\alpha, \bar{\phi} \rangle\} + \iota \alpha \|(\text{Id}/2 + \mathcal{K}_\Gamma)\phi\|_T^2 - \alpha^2 \langle \mathcal{V}_\Gamma p, \bar{p} \rangle.$$

Hence,  $\Im\{\langle \mathcal{A}_\Gamma(\phi, p_\alpha), (\bar{\phi}, \bar{p}_\alpha) \rangle\} = \alpha \|(\text{Id}/2 + \mathcal{K}_\Gamma)\phi\|_T^2 - \alpha^2 \Im\{\langle \bar{p}, \mathcal{V}_\Gamma p \rangle\}$ . If  $\Im\{\langle \bar{p}, \mathcal{V}_\Gamma p \rangle\} = 0$ , we can choose  $\alpha = 1$ . Otherwise,  $\Im\{\langle \bar{p}, \mathcal{V}_\Gamma p \rangle\} > 0$  and we can choose  $\alpha > 0$  satisfying  $\alpha < \|(\text{Id}/2 + \mathcal{K}_\Gamma)\phi\|_T^2 / \Im\{\langle \bar{p}, \mathcal{V}_\Gamma p \rangle\}$ . Then  $(\Phi, P) := (\phi, p_\alpha)$  yields a counterexample of Assumption (16).  $\square$

In the following, we are going to develop a discrete counterpart of the theory in [20] that will cover in particular the case where  $\mathcal{A}_\Gamma$  yields one of the previous FEM-BEM couplings, to reformulate Problem (11b). However, even when (11b) is well-posed, the corresponding variational formulation (17) can be ill-posed at some wavenumbers, called *spurious resonances*, due to the introduction of boundary integral operators, see e.g. [53]. Thus, several situations can occur:

- (17) is well-posed, then (17) will be rewritten as a substructured form with a trivial kernel. It can be the case of the three couplings (20), (21) and (22) if the wavenumber  $\tilde{k}$  does not match a spurious resonance.

- Assuming (16) and using Moore-Penrose pseudo-inverses, (17) will be rewritten as a substructured form with a trivial kernel, even when the operator attached to (17) admits a non-trivial kernel because of a spurious resonance. In this situation, the substructured formulation takes the form of “identity + contraction”. This is the case of the Costabel coupling (20).

These two situations are not mutually exclusive: for instance, the Costabel coupling (20) falls into both when the wavenumber is not a spurious resonance.

**Remark 3.6.**

*If the Costabel FEM-BEM coupling is applied, then for any value of  $\tilde{k}$  we can reconstruct a solution of Problem (11b) from a solution of the variational form (17). If the Johnson-Nédélec or Bielak-MacCamy FEM-BEM couplings are applied, then we can reconstruct a solution of Problem (11b) from a solution of the variational form (17) only when  $\tilde{k}$  does not match a spurious resonance.*

## 4 Discretization

Now we introduce notations related to the discretization of problems of the form (17). We shall assume that the polyhedral domain  $\Omega \subset \mathbb{R}^d$  is covered by a  $d$ -dimensional regular simplicial mesh  $\mathcal{T}_h^d(\Omega)$ , i.e. a collection of  $d$ -dimensional simplices:

$$\overline{\Omega} = \cup \{ \bar{\tau}, \tau \in \mathcal{T}_h^d(\Omega) \}.$$

Any polyhedral  $d$ -dimensional subdomain  $\Theta \subset \Omega$  will be said to *conform* to this mesh if there exists a sub-collection  $\mathcal{T}_h^d(\Theta) \subset \mathcal{T}_h^d(\Omega)$  such that  $\overline{\Theta} = \cup_{\tau \in \mathcal{T}_h^d(\Theta)} \bar{\tau}$ . Let us denote  $\mathcal{T}_h^{d-1}(\Omega)$  the collection of  $(d-1)$ -dimensional simplices that are faces of elements of  $\mathcal{T}_h^d(\Omega)$ . Any  $(d-1)$ -dimensional set  $\Upsilon \subset \overline{\Omega}$  is said to *conform* to  $\mathcal{T}_h^d(\Omega)$  if there exists a subcollection of faces  $\mathcal{T}_h^{d-1}(\Upsilon) \subset \mathcal{T}_h^{d-1}(\Omega)$  such that  $\overline{\Upsilon} = \cup_{\tau \in \mathcal{T}_h^{d-1}(\Upsilon)} \bar{\tau}$ . In particular, the boundary  $\partial\Theta$  of any conforming  $d$ -dimensional subset  $\Theta \subset \Omega$  is conforming. Next we consider the space of  $\mathbb{P}_k$ -Lagrange finite element functions

$$V_h(\Omega) := \{v \in \mathcal{C}^0(\overline{\Omega}), v|_{\tau} \in \mathbb{P}_k(\tau), \forall \tau \in \mathcal{T}_h^d(\Omega)\}.$$

We have  $V_h(\Omega) \subset H^1(\Omega)$ . For any  $d$ -dimensional or  $(d-1)$ -dimensional conforming subset  $\Theta \subset \Omega$ , we consider the corresponding  $\mathbb{P}_k$ -Lagrange finite element space  $V_h(\Theta) := \{v|_{\Theta}, v \in V_h(\Omega)\}$ . We will also need to consider the spaces

$$\begin{aligned} Q_h(\Gamma) &\subset H^{-1/2}(\Gamma), \quad \dim Q_h(\Gamma) < +\infty, \\ V_h(\Omega, \Gamma) &:= V_h(\Omega) \times Q_h(\Gamma). \end{aligned}$$

The subsequent analysis does not need any further assumption on  $Q_h(\Gamma)$ . The finite dimensional space  $V_h(\Omega, \Gamma)$  yields a Galerkin approximation of  $H^1(\Omega) \times H^{-1/2}(\Gamma)$ , which leads to the operator  $A_{\Omega \times \Gamma} : V_h(\Omega, \Gamma) \rightarrow V_h(\Omega, \Gamma)^*$  defined by

$$\begin{aligned} \langle A_{\Omega \times \Gamma}(u, p), (v, q) \rangle &:= \langle \mathcal{A}_{\Omega}(u), v \rangle + \langle \mathcal{A}_{\Gamma}(u|_{\Gamma}, p), (v|_{\Gamma}, q) \rangle, \\ \forall (u, p), (v, q) \in V_h(\Omega, \Gamma). \end{aligned}$$

The operator  $A_{\Omega \times \Gamma}$  is simply the matrix stemming from the Galerkin discretization of (17). Similarly, we consider  $\ell_{\Omega \times \Gamma} \in V_h(\Omega, \Gamma)^*$  defined by  $\langle \ell_{\Omega \times \Gamma}, (v, q) \rangle := \langle \ell_\Omega, v \rangle + \langle \ell_\Gamma, (v|_\Gamma, q) \rangle$  for all  $v \in V_h(\Omega)$ ,  $q \in Q_h(\Gamma)$ . Leaving (17) apart, from now on we shall focus on the discrete problem

$$(u, p) \in V_h(\Omega, \Gamma) \text{ and} \\ A_{\Omega \times \Gamma}(u, p) = \ell_{\Omega \times \Gamma}. \quad (23)$$

One of our goals is to develop a discrete counterpart of the theory presented in [20], and the starting point of this analysis will be (23).

We do not discard the possibility of a non-trivial kernel  $\text{Ker}(A_{\Omega \times \Gamma}) \neq \{0\}$ . If the wavenumber  $\kappa(\mathbf{x})$  is real-valued, this may occur for example when considering (13)-(14)-(23) or (13)-(15)-(23). This can also occur with FEM-BEM coupling, i.e. (13)-(20)-(23) and (13)-(21)-(23), when the wavenumber matches a spurious resonance. See the discussion at the end of Sections 2 and 3.

## 5 Domain decomposition

We now subdivide the domain  $\Omega$  into a finite collection of non-overlapping polyhedra  $\bar{\Omega} = \bar{\Omega}_1 \cup \dots \cup \bar{\Omega}_J$  with  $\Omega_j \cap \Omega_k = \emptyset$  for  $j \neq k$ , and assume that each  $\Omega_j$  conforms with the mesh  $\mathcal{T}_h(\Omega)$ . In practice, the generation of such a partition can easily be automated with the help of a graph partitioner. In the context of FEM-BEM coupling, already the case  $J = 1$  appears relevant. We shall denote  $\Gamma_j := \partial\Omega_j$  and  $\Sigma := \Gamma \cup \Gamma_1 \cup \dots \cup \Gamma_J$  the *skeleton* of the subdomain partition. In line with the notation of Section 4, we recall that  $V_h(\Gamma) := \{v|_\Gamma, v \in V_h(\Omega)\}$ ,  $V_h(\Sigma) := \{v|_\Sigma, v \in V_h(\Omega)\}$ ,  $V_h(\Gamma_j) := \{v|_{\Gamma_j}, v \in V_h(\Omega)\}$ , and  $V_h(\Omega_j) := \{v|_{\Omega_j}, v \in V_h(\Omega)\}$ . Next, we introduce function spaces adapted to the multi-domain setting:

$$\begin{aligned} V_h^B(\Gamma) &:= V_h(\Gamma) \times Q_h(\Gamma) \\ V_h(\Omega) &:= V_h^B(\Gamma) \times V_h(\Omega_1) \times \dots \times V_h(\Omega_J) \\ V_h(\Sigma) &:= V_h(\Gamma) \times V_h(\Gamma_1) \times \dots \times V_h(\Gamma_J). \end{aligned}$$

The space  $V_h(\Sigma)$  consists of independent tuples of Dirichlet traces on the boundary of each subdomain, and we shall refer to it as *Dirichlet multi-trace space*. Then, we introduce trace operators, beginning with  $\mathcal{B}: V_h(\Omega, \Gamma) \rightarrow V_h(\Sigma)$  defined by  $\mathcal{B}(v, q) := v|_\Sigma$ . We also consider a multi-domain boundary trace operator  $B: V_h(\Omega) \rightarrow V_h(\Sigma)$  that acts subdomain-wise and is block-diagonal:

$$\begin{aligned} B &:= \text{diag}(B_\Gamma, B_{\Omega_1}, \dots, B_{\Omega_J}) \\ B_\Gamma(v, q) &:= v \quad \text{and} \quad B_{\Omega_j}(u) := u|_{\Gamma_j}. \end{aligned}$$

In practice, the trace operators  $\mathcal{B}, B$  are made of Boolean matrices that keep track of the correspondence between volume degrees of freedom and boundary degrees of freedom. We also need restriction operators  $\mathcal{R}: V_h(\Omega, \Gamma) \rightarrow V_h(\Omega)$  and  $R: V_h(\Sigma) \rightarrow V_h(\Sigma)$  defined by

$$\begin{aligned} \mathcal{R}(v, q) &:= ((v|_\Gamma, q), v|_{\Omega_1}, \dots, v|_{\Omega_J}) \quad v \in V_h(\Omega), q \in Q_h(\Gamma) \\ R(u) &:= (u|_\Gamma, u|_{\Gamma_1}, \dots, u|_{\Gamma_J}) \quad u \in V_h(\Sigma). \end{aligned} \quad (24)$$

Here again, the restriction operators  $\mathcal{R}, R$  reduce to Boolean matrices encoding adjacency relation between subdomains or boundaries. They play a pivotal role in the expression of

transmission conditions. Note the commutativity relation  $R \cdot \mathcal{B} = \mathcal{B} \cdot \mathcal{R}$ . Next we need to introduce a notation for the range of the restriction operators

$$\begin{aligned}\mathbb{X}_h(\Omega) &:= \mathcal{R}(V_h(\Omega, \Gamma)), \\ \mathbb{X}_h(\Sigma) &:= R(V_h(\Sigma)).\end{aligned}\tag{25}$$

By construction,  $\mathbb{X}_h(\Omega) \subset \mathbb{V}_h(\Omega)$  and  $\mathbb{X}_h(\Sigma) \subset \mathbb{V}_h(\Sigma)$ . We call  $\mathbb{X}_h(\Sigma)$  the *Dirichlet single trace space*: it consists of tuples of Dirichlet traces that match across subdomain interfaces. Because this space encodes Dirichlet transmission conditions, it will play an important role in the subsequent analysis. Neumann transmission conditions are encoded by its annihilator  $\mathbb{X}_h(\Sigma)^\circ \subset \mathbb{V}_h(\Sigma)^*$ . The following two properties hold.

**Lemma 5.1.**

- i)  $\mathbb{X}_h(\Omega) = B^{-1}(\mathbb{X}_h(\Sigma))$ ,
- ii)  $\mathbb{X}_h(\Omega)^\circ = B^*(\mathbb{X}_h(\Sigma)^\circ)$ .

Here  $B^{-1}$  refers to a preimage, as  $B$  is not invertible. We do not provide the proof of this lemma as it follows exactly the same path as the one of [20, Lemma 4.1].

Let us now discuss in detail how we impose transmission conditions through interfaces. Our strategy requires a scalar product on the trace space, induced by an operator  $T$  called *impedance (or transmission) operator*:

$$\begin{aligned}T: \mathbb{V}_h(\Sigma) &\rightarrow \mathbb{V}_h(\Sigma)^* \quad \text{such that} \\ \langle T(\mathbf{u}), \bar{\mathbf{u}} \rangle &> 0, \quad \forall \mathbf{u} \in \mathbb{V}_h(\Sigma) \setminus \{0\} \quad \text{and} \quad T^* = T = \bar{T}.\end{aligned}\tag{26}$$

The above properties transfer to the inverse map  $T^{-1}: \mathbb{V}_h(\Sigma)^* \rightarrow \mathbb{V}_h(\Sigma)$  which itself induces a scalar product on  $\mathbb{V}_h(\Sigma)^*$ . We shall abundantly use the corresponding norms defined as follows:

$$\|\mathbf{v}\|_T^2 := \langle T(\mathbf{v}), \bar{\mathbf{v}} \rangle \quad \text{and} \quad \|\mathbf{p}\|_{T^{-1}}^2 := \langle T^{-1}(\mathbf{p}), \bar{\mathbf{p}} \rangle.$$

The following result, whose proof can be found in [21, Lemma 3.4], establishes a connection between the orthogonal complement of the single trace space and its annihilator.

**Lemma 5.2.**

For any impedance operator  $T: \mathbb{V}_h(\Sigma) \rightarrow \mathbb{V}_h(\Sigma)^*$  we have the two orthogonal decompositions

$$\begin{aligned}\mathbb{V}_h(\Sigma) &= \mathbb{X}_h(\Sigma) \oplus T^{-1}(\mathbb{X}_h(\Sigma)^\circ), \\ \mathbb{V}_h(\Sigma)^* &= \mathbb{X}_h(\Sigma)^\circ \oplus T(\mathbb{X}_h(\Sigma)).\end{aligned}$$

The space  $\mathcal{X}_h(\Sigma) := \mathbb{X}_h(\Sigma) \times \mathbb{X}_h(\Sigma)^\circ$  is a subspace of  $\mathcal{H}_h(\Sigma) := \mathbb{V}_h(\Sigma) \times \mathbb{V}_h(\Sigma)^*$  that provides a characterization of both Dirichlet and Neumann transmission conditions (note that they are satisfied by functions of the space  $V_h(\Omega, \Gamma)$  in the initial discrete problem (23)). The next result follows from Lemma 5.2 and is a further characterization of this subspace, established e.g. in [21, Lemma 3.5 and 3.7]. It reformulates Dirichlet/Neumann transmission conditions as *generalized impedance transmission conditions*.

**Lemma 5.3.**

Define  $\Pi: \mathbb{V}_h(\Sigma)^* \rightarrow \mathbb{V}_h(\Sigma)^*$  by  $\Pi := 2TR(R^*TR)^{-1}R^* - \text{Id}$ . Then  $\Pi$  is an involutive isometry, that is,  $\Pi^2 = \text{Id}$  and  $\|\Pi(\mathbf{q})\|_{T^{-1}} = \|\mathbf{q}\|_{T^{-1}}$ ,  $\forall \mathbf{q} \in \mathbb{V}_h(\Sigma)^*$ . Moreover, for any pair  $(\mathbf{v}, \mathbf{p}) \in \mathcal{H}_h(\Sigma) := \mathbb{V}_h(\Sigma) \times \mathbb{V}_h(\Sigma)^*$ , we have

$$(\mathbf{v}, \mathbf{p}) \in \mathcal{X}_h(\Sigma) := \mathbb{X}_h(\Sigma) \times \mathbb{X}_h(\Sigma)^\circ \iff -\mathbf{p} + iT(\mathbf{v}) = \Pi(\mathbf{p} + iT(\mathbf{v})).\tag{27}$$

This characterization of transmission conditions is non-trivial, even in the case of a single subdomain  $J = 1$ , i.e., if the computational domain  $\Omega$  is not subdivided. We name  $\Pi$  the *exchange operator*. The exact form taken by this operator intrinsically depends on the choice of the impedance operator  $T$ . The operator  $\Pi$  a priori couples distant subdomains, although, for certain choices of  $T$ , the exchange operator becomes local, that is, it couples only adjacent subdomain, see the discussion in [21, Section 9].

## 6 Substructured reformulation of the problem

We wish to reformulate Problem (23) considering the domain decomposition introduced in the previous section. Define the Galerkin discretization  $A_\Gamma: V_h^B(\Gamma) \rightarrow V_h^B(\Gamma)^*$  of the boundary operator  $\mathcal{A}_\Gamma$ , that is,  $\langle A_\Gamma(\mathbf{u}), \mathbf{v} \rangle := \langle \mathcal{A}_\Gamma(\mathbf{u}), \mathbf{v} \rangle$  for all  $\mathbf{u}, \mathbf{v} \in V_h^B(\Gamma)$ , and define the block-diagonal operator  $A: V_h(\Omega) \rightarrow V_h(\Omega)^*$  by

$$A := \text{diag}(A_\Gamma, A_{\Omega_1}, \dots, A_{\Omega_J})$$

$$\langle A_{\Omega_j}(\mathbf{u}), \mathbf{v} \rangle := \int_{\Omega_j} (\nabla \mathbf{u} \cdot \nabla \mathbf{v} - \kappa^2 \mathbf{u} \mathbf{v}) d\mathbf{x} \quad \forall \mathbf{u}, \mathbf{v} \in V_h(\Omega_j).$$

Due to Assumption (10) on the sign of the imaginary part of the problem under study, if Assumption (16) is also satisfied, then the block diagonal operator  $A$  itself satisfies a similar property

$$(10), (16) \implies \text{Im}\{\langle A(\mathbf{v}), \bar{\mathbf{v}} \rangle\} \leq 0, \quad \forall \mathbf{v} \in V_h(\Omega). \quad (28)$$

The source term of (23) can be decomposed similarly to  $A$ . We define  $\ell_{\Omega_j} \in V_h(\Omega_j)^*$  by  $\langle \ell_{\Omega_j}, \mathbf{v} \rangle := \int_{\Omega_j} f \mathbf{v} d\mathbf{x}$  for all  $\mathbf{v} \in V_h(\Omega_j)$ , and then  $\ell := (\ell_\Gamma, \ell_{\Omega_1}, \dots, \ell_{\Omega_J}) \in V_h(\Omega)^*$ . By definition of  $\mathcal{R}$  in (24), we have the factorizations

$$A_{\Omega \times \Gamma} = \mathcal{R}^* A \mathcal{R} \quad \text{and} \quad \ell_{\Omega \times \Gamma} = \mathcal{R}^* \ell. \quad (29)$$

The block-diagonal operator  $A$  can then be used to decompose Problem (23) subdomain-wise, and express the following first reformulation of Problem (23).

### Lemma 6.1.

If  $(\mathbf{u}, p) \in V_h(\Omega, \Gamma)$  satisfies Problem (23), then there exists  $\mathbf{p} \in V_h(\Sigma)^*$  such that, for  $\mathbf{u} = \mathcal{R}(\mathbf{u}, p)$ , the following equations hold

$$\begin{aligned} \mathbf{u} &\in V_h(\Omega), \mathbf{p} \in V_h(\Sigma)^* \\ A\mathbf{u} - B^*\mathbf{p} &= \ell \\ -\mathbf{p} + iTBu &= \Pi(\mathbf{p} + iTBu). \end{aligned} \quad (30)$$

Reciprocally if (30) holds for a pair  $(\mathbf{u}, \mathbf{p}) \in V_h(\Omega) \times V_h(\Sigma)^*$ , then there exists  $(\mathbf{u}, p) \in V_h(\Omega, \Gamma)$  solution to Problem (23) such that  $\mathbf{u} = \mathcal{R}(\mathbf{u}, p)$ .

*Proof.* Since by definition  $\mathbb{X}_h(\Omega) := \mathcal{R}(V_h(\Omega, \Gamma))$ , Equation (23) can be rewritten  $[\mathbf{u} := \mathcal{R}(\mathbf{u}, p) \in \mathbb{X}_h(\Omega) \text{ and } \langle A(\mathbf{u}) - \ell, \mathbf{v} \rangle = 0, \forall \mathbf{v} \in \mathbb{X}_h(\Omega)]$ , which is equivalent to  $[\mathbf{u} \in \mathbb{X}_h(\Omega) \text{ and } A(\mathbf{u}) - \ell \in \mathbb{X}_h(\Omega)^\circ]$ . Next we know from *i*) of Lemma 5.1 that  $[\mathbf{u} \in \mathbb{X}_h(\Omega)] \iff [\mathbf{u} \in V_h(\Omega) \text{ and } B(\mathbf{u}) \in \mathbb{X}_h(\Sigma)]$ , and *ii*) of Lemma 5.1 yields  $[\mathbf{A}(\mathbf{u}) - \ell \in \mathbb{X}_h(\Omega)^\circ] \iff [\exists \mathbf{p} \in \mathbb{X}_h(\Sigma)^\circ \text{ such that } A(\mathbf{u}) - \ell = B^*\mathbf{p}]$ . Thanks to the characterization of  $\mathcal{X}_h(\Sigma) = \mathbb{X}_h(\Sigma) \times \mathbb{X}_h(\Sigma)^\circ$  provided by Lemma 5.3, we finally obtain (30).  $\square$

We wish to further rearrange Problem (30), so as to eliminate the volume unknown  $\mathbf{u}$ , and reduce the problem to an equation with a substructured unknown on the skeleton  $\Sigma$  only. Following the theory in [21, 23], we rewrite the first equation of (30) as  $(\mathbf{A} - i\mathbf{B}^* \mathbf{T} \mathbf{B})\mathbf{u} = \mathbf{B}^*(\mathbf{p} - i\mathbf{T} \mathbf{B} \mathbf{u}) + \boldsymbol{\ell}$ . However, in the present case the operator  $\mathbf{A} - i\mathbf{B}^* \mathbf{T} \mathbf{B}$  may be singular, contrary to the situation in [21, 23]. Here are two fundamental properties that we will use to circumvent this state of affairs.

**Lemma 6.2.**

If either  $\mathbf{A} - i\mathbf{B}^* \mathbf{T} \mathbf{B}$  is invertible, or Assumption (16) holds, then

- i)  $\text{Ker}(\mathbf{A} - i\mathbf{B}^* \mathbf{T} \mathbf{B}) = \text{Ker}(\mathbf{A}) \cap \text{Ker}(\mathbf{B})$
- ii)  $\text{Im}(\mathbf{A} - i\mathbf{B}^* \mathbf{T} \mathbf{B}) = \text{Im}(\mathbf{A}) + \text{Im}(\mathbf{B}^*)$

*Proof.* The result is clear if  $\mathbf{A} - i\mathbf{B}^* \mathbf{T} \mathbf{B}$  is invertible. Indeed,  $\text{Ker}(\mathbf{A}) \cap \text{Ker}(\mathbf{B}) \subset \text{Ker}(\mathbf{A} - i\mathbf{B}^* \mathbf{T} \mathbf{B}) = \{0\}$  implies  $\text{Ker}(\mathbf{A}) \cap \text{Ker}(\mathbf{B}) = \{0\}$ , and  $\mathbb{V}_h(\Omega)^* = \text{Im}(\mathbf{A} - i\mathbf{B}^* \mathbf{T} \mathbf{B}) \subset \text{Im}(\mathbf{A}) + \text{Im}(\mathbf{B}^*)$  implies  $\text{Im}(\mathbf{A}) + \text{Im}(\mathbf{B}^*) = \mathbb{V}_h(\Omega)^*$ .

Let us assume now that  $\mathbf{A} - i\mathbf{B}^* \mathbf{T} \mathbf{B}$  has a non-trivial kernel, but Assumption (16) holds, which implies (28):  $\Im\{\langle \mathbf{A}(\mathbf{v}), \bar{\mathbf{v}} \rangle\} \leq 0$ ,  $\forall \mathbf{v} \in \mathbb{V}_h(\Omega)$ . On the one hand,  $\text{Ker}(\mathbf{A}) \cap \text{Ker}(\mathbf{B}) \subset \text{Ker}(\mathbf{A} - i\mathbf{B}^* \mathbf{T} \mathbf{B})$ . On the other hand,  $\mathbf{u} \in \text{Ker}(\mathbf{A} - i\mathbf{B}^* \mathbf{T} \mathbf{B}) \Rightarrow 0 = \Im\{\langle \mathbf{A}(\mathbf{u}), \bar{\mathbf{u}} \rangle - i\langle \mathbf{B}^* \mathbf{T} \mathbf{B}(\mathbf{u}), \bar{\mathbf{u}} \rangle\} = \Im\{\langle \mathbf{A}(\mathbf{u}), \bar{\mathbf{u}} \rangle\} - \|\mathbf{B}(\mathbf{u})\|_{\mathbf{T}}^2$ , so that  $0 \leq \|\mathbf{B}(\mathbf{u})\|_{\mathbf{T}}^2 = \Im\{\langle \mathbf{A}(\mathbf{u}), \bar{\mathbf{u}} \rangle\} \leq 0 \Rightarrow \mathbf{B}(\mathbf{u}) = 0 \Rightarrow \mathbf{u} \in \text{Ker}(\mathbf{B})$ . Finally,  $\mathbf{u} \in \text{Ker}(\mathbf{A} - i\mathbf{B}^* \mathbf{T} \mathbf{B}) \cap \text{Ker}(\mathbf{B}) = \text{Ker}(\mathbf{A}) \cap \text{Ker}(\mathbf{B})$ . This establishes i).

Since  $\Im\{\langle \mathbf{A}^*(\bar{\mathbf{v}}), \mathbf{v} \rangle\} = \Im\{\langle \mathbf{A}(\mathbf{v}), \bar{\mathbf{v}} \rangle\} \leq 0$ ,  $\forall \mathbf{v} \in \mathbb{V}_h(\Omega)$ , we prove in the same manner that  $\text{Ker}(\mathbf{A}^* - i\mathbf{B}^* \mathbf{T} \mathbf{B}) = \text{Ker}(\mathbf{A}^*) \cap \text{Ker}(\mathbf{B})$ . Hence, using (6) and (4),  $\text{Im}(\mathbf{A}) + \text{Im}(\mathbf{B}^*) = \text{Ker}(\mathbf{A}^*)^\circ + \text{Ker}(\mathbf{B})^\circ = (\text{Ker}(\mathbf{A}^*) \cap \text{Ker}(\mathbf{B}))^\circ = \text{Ker}(\mathbf{A}^* - i\mathbf{B}^* \mathbf{T} \mathbf{B})^\circ = \text{Im}(\mathbf{A} - i\mathbf{B}^* \mathbf{T} \mathbf{B})$ .  $\square$

**Remark 6.3.**

Under one of the hypotheses of Lemma 6.2, if (30) holds, then  $\boldsymbol{\ell} \in \text{Im}(\mathbf{A} - i\mathbf{B}^* \mathbf{T} \mathbf{B})$  necessarily.

**Remark 6.4.**

In the following, we will use the relations i) and ii) of Lemma 6.2. Thus, our discrete theory will cover both the case when  $\mathbf{A} - i\mathbf{B}^* \mathbf{T} \mathbf{B}$  has a non-trivial kernel, and when it is invertible. In the latter case, proofs could be simplified using the stronger result that  $\text{Ker}(\mathbf{A} - i\mathbf{B}^* \mathbf{T} \mathbf{B}) = \{0\}$  and  $\text{Im}(\mathbf{A} - i\mathbf{B}^* \mathbf{T} \mathbf{B})$  is the whole discrete space.

Like in [20, 21, 23], the rearrangement of Problem (30) will rely on pairs of Dirichlet-Neumann traces. This leads us to introduce the multi-trace space

$$\begin{aligned} \mathcal{H}_h(\Sigma) &:= \mathbb{V}_h(\Sigma) \times \mathbb{V}_h(\Sigma)^* \\ \|(\mathbf{v}, \mathbf{p})\|_{\mathbf{T} \times \mathbf{T}^{-1}}^2 &:= \|\mathbf{v}\|_{\mathbf{T}}^2 + \|\mathbf{p}\|_{\mathbf{T}^{-1}}^2. \end{aligned}$$

Two subspaces of  $\mathcal{H}_h(\Sigma)$  will play a pivotal role. They are related to local problems and transmission conditions, and defined as follows

$$\begin{aligned} \mathcal{C}_h(\mathbf{A}) &:= \{(\mathbf{B}(\mathbf{u}), \mathbf{p}) \in \mathcal{H}_h(\Sigma), \mathbf{A}\mathbf{u} = \mathbf{B}^*\mathbf{p}\}, \\ \mathcal{X}_h(\Sigma) &:= \mathbb{X}_h(\Sigma) \times \mathbb{X}_h(\Sigma)^\circ, \end{aligned} \tag{31}$$

where  $\mathcal{C}_h(\mathbf{A})$  is often called the *Cauchy data* set. The single-trace space  $\mathcal{X}_h(\Sigma)$  was already introduced in Lemma 5.3 and characterized using the exchange operator  $\Pi$ . We have the following fundamental results involving the space  $\mathcal{C}_h(\mathbf{A})$ .

### Proposition 6.5.

Under one of the hypotheses of Lemma 6.2, the application  $(\mathbf{v}, \mathbf{p}) \mapsto \mathbf{p} - iT(\mathbf{v})$  isomorphically maps  $\mathcal{C}_h(\mathbf{A})$  onto  $\mathbb{V}_h(\Sigma)^*$ , with the estimate  $\|(\mathbf{v}, \mathbf{p})\|_{T \times T^{-1}}^2 \leq \|\mathbf{p} - iT\mathbf{v}\|_{T^{-1}}^2 \leq 2 \|(\mathbf{v}, \mathbf{p})\|_{T \times T^{-1}}^2$  for all  $(\mathbf{v}, \mathbf{p}) \in \mathcal{C}_h(\mathbf{A})$ .

*Proof.* Pick  $\mathbf{q} \in \mathbb{V}_h(\Sigma)^*$  arbitrary. According to *ii*) of Lemma 6.2, there exists  $\mathbf{u} \in \mathbb{V}_h(\Omega)$  such that  $(\mathbf{A} - i\mathbf{B}^* \mathbf{T} \mathbf{B})\mathbf{u} = \mathbf{B}^* \mathbf{q}$ , which rewrites  $\mathbf{A}\mathbf{u} = \mathbf{B}^*(\mathbf{q} + iT\mathbf{B}\mathbf{u})$ . As a consequence  $(\mathbf{v}, \mathbf{p}) := (\mathbf{B}\mathbf{u}, \mathbf{q} + iT\mathbf{B}\mathbf{u}) \in \mathcal{C}_h(\mathbf{A})$ , and  $\mathbf{p} - iT\mathbf{v} = \mathbf{q}$  by construction, hence the surjectivity.

Next, for any  $(\mathbf{v}, \mathbf{p}) \in \mathcal{C}_h(\mathbf{A})$ , there exists  $\mathbf{u} \in \mathbb{V}_h(\Omega)$  such that  $\mathbf{v} = \mathbf{B}\mathbf{u}$  and  $\mathbf{B}^* \mathbf{p} = \mathbf{A}\mathbf{u}$ . Thus,  $\langle \mathbf{p}, \bar{\mathbf{v}} \rangle = \langle \mathbf{p}, \mathbf{B}(\bar{\mathbf{u}}) \rangle = \langle \mathbf{B}^*(\mathbf{p}), \bar{\mathbf{u}} \rangle = \langle \mathbf{A}(\mathbf{u}), \bar{\mathbf{u}} \rangle$ . Then, (28) yields  $0 \leq -2\Im\{\langle \mathbf{p}, \bar{\mathbf{v}} \rangle\} \leq \|(\mathbf{v}, \mathbf{p})\|_{T \times T^{-1}}^2$ , hence  $0 \leq \|\mathbf{p} - iT\mathbf{v}\|_{T^{-1}}^2 - \|(\mathbf{v}, \mathbf{p})\|_{T \times T^{-1}}^2 \leq \|(\mathbf{v}, \mathbf{p})\|_{T \times T^{-1}}^2$ , which establishes both injectivity and the estimates.  $\square$

### Proposition 6.6.

Assume one of the hypotheses of Lemma 6.2. Define the graph space of  $iT: \mathbb{V}_h(\Sigma) \rightarrow \mathbb{V}_h(\Sigma)^*$ :  $\mathcal{G}(iT) := \{(\mathbf{v}, iT(\mathbf{v})), \mathbf{v} \in \mathbb{V}_h(\Sigma)\}$ . Then

$$\mathcal{H}_h(\Sigma) = \mathcal{C}_h(\mathbf{A}) \oplus \mathcal{G}(iT).$$

*Proof.* Let  $(\mathbf{v}, \mathbf{p}) \in \mathcal{C}_h(\mathbf{A}) \cap \mathcal{G}(iT)$ . There exists  $\mathbf{u} \in \mathbb{V}_h(\Omega)$  such that  $\mathbf{v} = \mathbf{B}(\mathbf{u})$ ,  $\mathbf{A}\mathbf{u} = \mathbf{B}^* \mathbf{p}$ , and  $\mathbf{p} = iT\mathbf{v}$ . Combining these relations with Lemma 6.2, we deduce that  $\mathbf{u} \in \text{Ker}(\mathbf{A} - i\mathbf{B}^* \mathbf{T} \mathbf{B}) = \text{Ker}(\mathbf{A}) \cap \text{Ker}(\mathbf{B})$ , and then  $(\mathbf{v}, \mathbf{p}) = (0, 0)$ .

Now take an arbitrary  $(\mathbf{v}, \mathbf{p}) \in \mathcal{H}_h(\Sigma)$ . By surjectivity of  $\mathbf{B}$ , there exists  $\tilde{\mathbf{u}} \in \mathbb{V}_h(\Omega)$  such that  $\mathbf{B}(\tilde{\mathbf{u}}) = \mathbf{v}$ . Using *ii*) of Lemma 6.2, we deduce that there exists  $\mathbf{w} \in \mathbb{V}_h(\Omega)$  such that  $(\mathbf{A} - i\mathbf{B}^* \mathbf{T} \mathbf{B})\mathbf{w} = \mathbf{A}\tilde{\mathbf{u}} - \mathbf{B}^* \mathbf{p}$ . Set

$$\begin{aligned} \mathbf{v}_1 &:= \mathbf{B}(\mathbf{w}), & \mathbf{p}_1 &:= iT\mathbf{v}_1 = iT\mathbf{B}(\mathbf{w}), \\ \mathbf{v}_2 &:= \mathbf{B}(\tilde{\mathbf{u}} - \mathbf{w}), & \mathbf{p}_2 &:= \mathbf{p} - iT\mathbf{B}(\mathbf{w}). \end{aligned}$$

By construction,  $(\mathbf{v}_1, \mathbf{p}_1) \in \mathcal{G}(iT)$ . Besides,  $\mathbf{A}(\tilde{\mathbf{u}} - \mathbf{w}) = \mathbf{B}^*(\mathbf{p} - iT\mathbf{B}\mathbf{w}) = \mathbf{B}^* \mathbf{p}_2$ , so that  $(\mathbf{v}_2, \mathbf{p}_2) \in \mathcal{C}_h(\mathbf{A})$ . To end the proof, note that  $\mathbf{v}_1 + \mathbf{v}_2 = \mathbf{B}(\tilde{\mathbf{u}}) = \mathbf{v}$  and  $\mathbf{p}_1 + \mathbf{p}_2 = \mathbf{p}$  so that  $\mathcal{C}_h(\mathbf{A}) + \mathcal{G}(iT) = \mathcal{H}_h(\Sigma)$ .  $\square$

The space  $\mathcal{C}_h(\mathbf{A})$  introduced above “models” the wave equation local to each subdomain. In the next Proposition, we introduce the so-called *scattering operator*, which will play the role of a local solver in our domain decomposition method. Recall the definition of the Moore-Penrose pseudo-inverse mentioned in Section 1 and denoted with  $\dagger$ .

### Proposition 6.7.

Assume one of the hypotheses of Lemma 6.2. There exists a unique linear map  $\mathbf{S}: \mathbb{V}_h(\Sigma)^* \rightarrow \mathbb{V}_h(\Sigma)^*$ , later referred to as scattering operator, that satisfies

$$\mathbf{p} + iT\mathbf{v} = \mathbf{S}(\mathbf{p} - iT\mathbf{v}), \quad \forall (\mathbf{v}, \mathbf{p}) \in \mathcal{C}_h(\mathbf{A}). \quad (32)$$

This operator is also given by the formula  $\mathbf{S} = \text{Id} + 2iT\mathbf{B}(\mathbf{A} - i\mathbf{B}^* \mathbf{T} \mathbf{B})^\dagger \mathbf{B}^*$ .

Besides, assuming (16),  $\mathbf{S}$  is  $T^{-1}$ -contractive<sup>2</sup>, i.e. for any  $\mathbf{q} \in \mathbb{V}_h(\Sigma)^*$ ,  $\|\mathbf{S}(\mathbf{q})\|_{T^{-1}} \leq \|\mathbf{q}\|_{T^{-1}}$ . More precisely,

$$\begin{aligned} \|\mathbf{S}(\mathbf{q})\|_{T^{-1}}^2 - 4\Im\{\langle \mathbf{A}(\mathbf{u}), \bar{\mathbf{u}} \rangle\} &= \|\mathbf{q}\|_{T^{-1}}^2 \\ \text{where } \mathbf{u} &= (\mathbf{A} - i\mathbf{B}^* \mathbf{T} \mathbf{B})^\dagger \mathbf{B}^* \mathbf{q}. \end{aligned} \quad (33)$$

*Proof.* Proposition 6.5 shows that Equation (32) unequivocally defines the operator  $S$ . Next, pick  $\mathbf{q} \in \mathbb{V}_h(\Sigma)^*$  arbitrary. According to *ii*) of Lemma 6.2, there exists  $\tilde{\mathbf{u}} \in \mathbb{V}_h(\Omega)$  such that  $(A - iB^*TB)\tilde{\mathbf{u}} = B^*\mathbf{q}$ . Let us set  $\mathbf{u} := (A - iB^*TB)^\dagger(A - iB^*TB)\tilde{\mathbf{u}}$ . Then, according to the standard properties of Moore-Penrose pseudo-inverse  $M \cdot M^\dagger \cdot M = M$ , with  $M = A - iB^*TB$ . So, we conclude  $(A - iB^*TB)\mathbf{u} = (A - iB^*TB)\tilde{\mathbf{u}} = B^*\mathbf{q}$ .

Now set  $\mathbf{p} = \mathbf{q} + iTB\mathbf{u}$ . We have  $A\mathbf{u} - B^*\mathbf{p} = 0$  hence  $(B\mathbf{u}, \mathbf{p}) \in \mathcal{C}_h(A)$ . Since  $\mathbf{q} = \mathbf{p} - iTB\mathbf{u}$ , Equation (32) gives  $S(\mathbf{q}) = \mathbf{p} + iTB\mathbf{u} = \mathbf{q} + 2iT\mathbf{u} = (\text{Id} + 2iT(B - iB^*TB)^\dagger B^*)\mathbf{q}$  for all  $\mathbf{q} \in \mathbb{V}_h(\Sigma)^*$ , which confirms the alternative expression of  $S$  stated above. The contractivity identity (33) is established as follows

$$\begin{aligned} \|S(\mathbf{q})\|_{T^{-1}}^2 &= \|\mathbf{q} + 2iT\mathbf{u}\|_{T^{-1}}^2 \\ &= \|\mathbf{q}\|_{T^{-1}}^2 + 4\|B\mathbf{u}\|_T^2 + 4\Im\{\langle \mathbf{q}, B\bar{\mathbf{u}} \rangle\} \\ &= \|\mathbf{q}\|_{T^{-1}}^2 + 4\|B\mathbf{u}\|_T^2 + 4\Im\{\langle A\mathbf{u}, \bar{\mathbf{u}} \rangle\} - 4\Im\{i\langle B^*TB\mathbf{u}, \bar{\mathbf{u}} \rangle\} \\ &= \|\mathbf{q}\|_{T^{-1}}^2 + 4\Im\{\langle A\mathbf{u}, \bar{\mathbf{u}} \rangle\}. \end{aligned}$$

□

The scattering operator actually gives a characterization of the space of Cauchy data  $\mathcal{C}_h(A)$ .

### Lemma 6.8.

Assume one of the hypotheses of Lemma 6.2. For any  $(\mathbf{v}, \mathbf{p}) \in \mathcal{H}_h(\Sigma)$

$$(\mathbf{v}, \mathbf{p}) \in \mathcal{C}_h(A) \iff \mathbf{p} + iT\mathbf{v} = S(\mathbf{p} - iT\mathbf{v}).$$

*Proof.* The proof relies on (32) and Proposition 6.6, and is similar to the one in [20, Lemma 7.3]. □

We can now continue with the reformulation of Problem (30).

### Proposition 6.9.

Assume one of the hypotheses of Lemma 6.2. If  $(\mathbf{u}, \mathbf{p}) \in \mathbb{V}_h(\Omega) \times \mathbb{V}_h(\Sigma)^*$  satisfies (30) for some  $\ell \in \text{Im}(A) + \text{Im}(B^*)$ , then the pair  $(\mathbf{q}_+, \mathbf{q}_-) := (\mathbf{p} + iTB\mathbf{u}, \mathbf{p} - iTB\mathbf{u}) \in \mathbb{V}_h(\Sigma)^* \times \mathbb{V}_h(\Sigma)^*$  satisfies

$$\begin{aligned} \mathbf{q}_+ - S(\mathbf{q}_-) &= 2iT(B - iB^*TB)^\dagger \ell \\ \Pi(\mathbf{q}_+) + \mathbf{q}_- &= 0. \end{aligned} \tag{34}$$

Conversely, if  $(\mathbf{q}_+, \mathbf{q}_-) \in \mathbb{V}_h(\Sigma)^* \times \mathbb{V}_h(\Sigma)^*$  satisfies (34) for some  $\ell \in \text{Im}(A) + \text{Im}(B^*)$ , then the pair  $(\mathbf{u}, \mathbf{p}) \in \mathbb{V}_h(\Omega) \times \mathbb{V}_h(\Sigma)^*$ , given by  $\mathbf{u} = (A - iB^*TB)^\dagger(B^*\mathbf{q}_- + \ell)$  and  $\mathbf{p} = (\mathbf{q}_+ + \mathbf{q}_-)/2$ , solves (30).

*Proof.* If  $(\mathbf{u}, \mathbf{p}) \in \mathbb{V}_h(\Omega) \times \mathbb{V}_h(\Sigma)^*$  satisfies (30), let us set  $\mathbf{q}_\pm = \mathbf{p} \pm iTB(\mathbf{u})$  and  $\mathbf{g} = 2iT(B - iB^*TB)^\dagger \ell$ . Then, the second equation of (30) readily implies  $\Pi(\mathbf{q}_+) + \mathbf{q}_- = 0$ . On the other hand, rearranging the terms in the first equation of (30) yields  $(A - iB^*TB)\mathbf{u} = B^*\mathbf{q}_- + \ell$ , which can be multiplied by  $(A - iB^*TB)^\dagger$ . Since  $\text{Ker}(A - iB^*TB) \subset \text{Ker}(B)$  according to Lemma 6.2, using (iii) from (7) and (8b) we obtain  $B(\mathbf{u}) = B(A - iB^*TB)^\dagger(A - iB^*TB)\mathbf{u} = B(A - iB^*TB)^\dagger(B^*\mathbf{q}_- + \ell)$ . Then, using the expression of the scattering operator provided by Proposition 6.7, this yields  $\mathbf{q}_- + 2iT\mathbf{u} = S(\mathbf{q}_-) + \mathbf{g}$ , which rewrites  $\mathbf{q}_+ = S(\mathbf{q}_-) + \mathbf{g}$ .

Now assume that  $(\mathbf{q}_+, \mathbf{q}_-) \in \mathbb{V}_h(\Sigma)^* \times \mathbb{V}_h(\Sigma)^*$  satisfies (34). Setting  $\mathbf{u} := (A - iB^*TB)^\dagger(B^*\mathbf{q}_- + \ell)$ , the first line of (34) indicates  $\mathbf{q}_+ - \mathbf{q}_- = 2iT\mathbf{u}$  and, with  $\mathbf{p} := (\mathbf{q}_+ + \mathbf{q}_-)/2$ , this yields

$\mathbf{q}_\pm = \mathbf{p} \pm i\mathbf{TB}(\mathbf{u})$ . Hence, from the second line of (34) we deduce  $\Pi(\mathbf{p} + i\mathbf{TB}\mathbf{u}) + \mathbf{p} - i\mathbf{TB}\mathbf{u} = 0$ . Next, since  $\mathbf{B}^* \mathbf{q}_- + \boldsymbol{\ell} \in \text{Im}(\mathbf{A}) + \text{Im}(\mathbf{B}^*) = \text{Im}(\mathbf{A} - i\mathbf{B}^*\mathbf{TB})$  by Lemma 6.2, using (iv) from (7) and (8a) we obtain  $(\mathbf{A} - i\mathbf{B}^*\mathbf{TB})\mathbf{u} = (\mathbf{A} - i\mathbf{B}^*\mathbf{TB})(\mathbf{A} - i\mathbf{B}^*\mathbf{TB})^\dagger(\mathbf{B}^* \mathbf{q}_- + \boldsymbol{\ell}) = \mathbf{B}^* \mathbf{q}_- + \boldsymbol{\ell}$ , which rewrites  $\mathbf{A}\mathbf{u} = \mathbf{B}^*(\mathbf{q}_- + i\mathbf{TB}\mathbf{u}) + \boldsymbol{\ell} = \mathbf{B}^*(\mathbf{p}) + \boldsymbol{\ell}$ . So  $(\mathbf{u}, \mathbf{p})$  solves Problem (30).  $\square$

### Remark 6.10.

The assumption  $\boldsymbol{\ell} \in \text{Im}(\mathbf{A}) + \text{Im}(\mathbf{B}^*)$  should not be regarded as a limitation of the present analysis since Problem (30) can only hold under such a condition.

Proposition 6.9 above has exhibited a reformulation of (30) as a  $2 \times 2$  system of equations posed only on the skeleton  $\Sigma$  of the subdomain partition. Left multiplying the first equation of (34) by  $\Pi$ , and using the second equation to write  $\mathbf{q}_- = -\Pi(\mathbf{q}_+)$ , we obtain the final substructured discrete formulation of our Helmholtz problem:

**Corollary 6.11** (Generalized Optimized Schwarz Method).

Assume one of the hypotheses of Lemma 6.2. If  $(\mathbf{u}, \mathbf{p}) \in \mathbb{V}_h(\Omega) \times \mathbb{V}_h(\Sigma)^*$  satisfies (30) for some  $\boldsymbol{\ell} \in \text{Im}(\mathbf{A}) + \text{Im}(\mathbf{B}^*)$ , then  $\mathbf{q} = \mathbf{p} - i\mathbf{TB}\mathbf{u}$  solves the problem

$$\begin{aligned} \mathbf{q} &\in \mathbb{V}_h(\Sigma)^* \quad \text{and} \\ (\text{Id} + \Pi S)\mathbf{q} &= -2i\Pi\mathbf{TB}(\mathbf{A} - i\mathbf{B}^*\mathbf{TB})^\dagger\boldsymbol{\ell} \end{aligned} \tag{35}$$

Conversely, if  $\mathbf{q}$  satisfies (35), then the pair  $(\mathbf{u}, \mathbf{p}) \in \mathbb{V}_h(\Omega) \times \mathbb{V}_h(\Sigma)^*$  given by  $\mathbf{u} = (\mathbf{A} - i\mathbf{B}^*\mathbf{TB})^\dagger(\mathbf{B}^* \mathbf{q} + \boldsymbol{\ell})$  and  $\mathbf{p} = (\mathbf{q} - \Pi(\mathbf{q}))/2$  solves (30).

Problem (35) is the GOSM formulation, with an unknown  $\mathbf{q}$  on the skeleton  $\Sigma$  of the domain partition. Let us underline the structure of the operator  $\text{Id} + \Pi S$  appearing in the left-hand side of (35). Since both  $\Pi$  and  $S$  are contractions<sup>2</sup> (see Lemma 5.3 and Proposition 6.7) when Assumption (16) holds, the operator  $\Pi S$  is itself a contraction and the operator  $\text{Id} + \Pi S$  takes the form of “identity + contraction”. This guarantees the positivity for this operator, a desirable property in the perspective of the iterative solver defined in Algorithm 1.

## 7 Analysis of resonances

As already pointed out at the end of Section 4, the operator  $\mathbf{A}_{\Omega \times \Gamma}$  of Formulation (23), that describes our boundary value problem, is not necessarily invertible. This may occur when modelling physical resonance phenomena, but may also occur in the case of spurious resonances stemming from a FEM-BEM coupling, as discussed at the end of Section 3. In the present section, we shall investigate how this situation transfers to our domain decomposition skeleton formulation (35). Our analysis is based on an intermediary map  $\Phi$  that we study in detail.

The next result involves  $\mathbf{B}^\dagger: \mathbb{V}_h(\Sigma) \rightarrow \mathbb{V}_h(\Omega)$ , which is called *harmonic lifting map* in the literature on domain decomposition (see e.g. [57, §4.4] or [47, §1.2.6]). We remind that  $\mathbf{B}^\dagger$  is the Moore-Penrose pseudo-inverse of the (surjective) trace map  $\mathbf{B}: \mathbb{V}_h(\Omega) \rightarrow \mathbb{V}_h(\Sigma)$ , see Section 1 and in particular (9) for a characterization.

### Proposition 7.1.

Assume one of the hypotheses of Lemma 6.2. Define the operator  $\Phi: \text{Ker}(\mathbf{A}_{\Omega \times \Gamma}) \rightarrow \mathbb{V}_h(\Sigma)^*$

by the formula  $\Phi(\mathbf{u}) := (B^\dagger)^* \cdot (A - iB^*TB) \cdot \mathcal{R}(\mathbf{u})$ . Then  $\mathbf{u} \in \text{Ker}(\Phi) \iff \mathcal{R}(\mathbf{u}) \in \text{Ker}(A) \cap \text{Ker}(B)$ , and  $\dim \text{Ker}(\Phi) = \dim(\text{Ker}(A) \cap \text{Ker}(B))$ .

*Proof.* Suppose first that  $\mathbf{u} = (u, p) \in \text{Ker}(A_{\Omega \times \Gamma})$  is arbitrary. We have  $\mathcal{R}(\mathbf{u}) \in \text{Im}(\mathcal{R}) = \mathbb{X}_h(\Omega)$  by (25) and  $A\mathcal{R}(\mathbf{u}) \in \text{Ker}(\mathcal{R}^*) = \mathbb{X}_h(\Omega)^\circ$  by (29) and (5). According to *ii*) of Lemma 5.1, there exists  $\mathbf{p} \in \mathbb{X}_h(\Sigma)^\circ$  such that  $A\mathcal{R}(\mathbf{u}) = B^*(\mathbf{p})$ . Then, setting  $\mathbf{v} = B\mathcal{R}(\mathbf{u}) \in \mathbb{X}_h(\Sigma) = B(\mathbb{X}_h(\Omega))$  by *i*) of Lemma 5.1,  $(\mathbf{v}, \mathbf{p}) \in \mathcal{C}_h(A) \cap \mathcal{X}_h(\Sigma)$  — see (31). Besides,  $(B^\dagger)^*A\mathcal{R}(\mathbf{u}) = (B^\dagger)^*B^*(\mathbf{p}) = (B \cdot B^\dagger)^*(\mathbf{p}) = \mathbf{p}$ , since  $B$  is surjective. This leads to

$$\Phi(\mathbf{u}) = \mathbf{p} - iT(\mathbf{v}). \quad (36)$$

Since  $(\mathbf{v}, \mathbf{p}) \in \mathcal{C}_h(A)$  and Proposition 6.5 holds, we derive  $\mathbf{u} \in \text{Ker}(\Phi) \iff \mathbf{p} - iT(\mathbf{v}) = 0 \iff (\mathbf{v}, \mathbf{p}) = 0$ . By the very definition of  $\mathbf{v}$  and  $\mathbf{p}$  above, and since  $B^* : \mathbb{V}_h(\Sigma)^* \rightarrow \mathbb{V}_h(\Omega)^*$  is one-to-one, we have  $(\mathbf{v}, \mathbf{p}) = 0 \iff [\mathbf{v} = 0 = B\mathcal{R}(\mathbf{u}) \text{ and } B^*(\mathbf{p}) = 0 = A\mathcal{R}(\mathbf{u})] \iff \mathcal{R}(\mathbf{u}) \in \text{Ker}(A) \cap \text{Ker}(B)$ .

We finish the proof by noting that  $\mathcal{R} : \mathbb{V}_h(\Omega, \Gamma) \rightarrow \mathbb{V}_h(\Omega)$  is one-to-one according to its definition (24), hence  $\dim \text{Ker}(\Phi) = \dim \mathcal{R}(\text{Ker}(\Phi)) = \dim(\text{Ker}(A) \cap \text{Ker}(B))$ .  $\square$

We underline that, in the previous result, the map  $\Phi$  is taken restricted to  $\text{Ker}(A_{\Omega \times \Gamma})$ . After having studied the kernel of this map, we now study its range.

### Proposition 7.2.

Assume one of the hypotheses of Lemma 6.2. Let  $\Phi$  be the operator defined in Proposition 7.1. Then  $\text{Im}(\Phi) = \Phi(\text{Ker}(A_{\Omega \times \Gamma})) = \text{Ker}(\text{Id} + \Pi S)$ .

*Proof.* Recall the description of the map  $\Phi$  from the beginning of the proof of Proposition 7.1 and (36). What precedes shows that, if  $\mathbf{u} \in \text{Ker}(A_{\Omega \times \Gamma})$ , then  $\Phi(\mathbf{u}) = \mathbf{p} - iT(\mathbf{v})$  for some  $(\mathbf{v}, \mathbf{p}) \in \mathcal{C}_h(A) \cap \mathcal{X}_h(\Sigma)$ . Applying the definition of the scattering operator  $S$ , see (32),  $S \cdot \Phi(\mathbf{u}) = \mathbf{p} + iT(\mathbf{v})$ . Then, applying the characterization of  $\mathcal{X}_h(\Sigma)$  with the exchange operator  $\Pi$ , see (27), we obtain  $\Pi \cdot S \cdot \Phi(\mathbf{u}) = \Pi(\mathbf{p} + iT(\mathbf{v})) = -\mathbf{p} + iT(\mathbf{v}) = -\Phi(\mathbf{u})$ . Hence,  $(\text{Id} + \Pi S)\Phi(\mathbf{u}) = 0$  for all  $\mathbf{u} \in \text{Ker}(A_{\Omega \times \Gamma})$ , which rewrites

$$\Phi(\text{Ker}(A_{\Omega \times \Gamma})) \subset \text{Ker}(\text{Id} + \Pi S).$$

There only remains to show that  $\Phi(\text{Ker}(A_{\Omega \times \Gamma})) \supset \text{Ker}(\text{Id} + \Pi S)$ . Pick an arbitrary  $\mathbf{q}_- \in \text{Ker}(\text{Id} + \Pi S)$  and set  $\mathbf{q}_+ = S(\mathbf{q}_-)$ . Since  $(\text{Id} + \Pi S)\mathbf{q}_- = 0$  we conclude that  $\mathbf{q}_- + \Pi(\mathbf{q}_+) = 0$ . Next define  $(\mathbf{v}, \mathbf{p}) \in \mathbb{V}_h(\Sigma) \times \mathbb{V}_h(\Sigma)^*$  by

$$\begin{cases} \mathbf{p} - iT\mathbf{v} = \mathbf{q}_- \\ \mathbf{p} + iT\mathbf{v} = \mathbf{q}_+ \end{cases} \iff \begin{cases} \mathbf{v} = T^{-1}(\mathbf{q}_+ - \mathbf{q}_-)/(2i) \\ \mathbf{p} = (\mathbf{q}_+ + \mathbf{q}_-)/2 \end{cases}.$$

According to the equations satisfied by  $(\mathbf{q}_-, \mathbf{q}_+)$ , we have  $\mathbf{p} + iT\mathbf{v} = S(\mathbf{p} - iT\mathbf{v})$  and  $-\mathbf{p} + iT\mathbf{v} = \Pi(\mathbf{p} + iT\mathbf{v})$ , which rewrites  $(\mathbf{v}, \mathbf{p}) \in \mathcal{C}_h(A) \cap \mathcal{X}_h(\Sigma)$  due to (27) and Lemma 6.8. Since  $(\mathbf{v}, \mathbf{p}) \in \mathcal{C}_h(A)$ , there exists  $\mathbf{w} \in \mathbb{V}_h(\Omega)$  such that  $B(\mathbf{w}) = \mathbf{v}$  and  $A\mathbf{w} = B^*(\mathbf{p})$ . On the other hand, as  $\mathbf{v} \in \mathbb{X}_h(\Sigma)$ , we derive  $\mathbf{w} \in B^{-1}(\mathbb{X}_h(\Sigma)) = \mathbb{X}_h(\Omega) = \mathcal{R}(\mathbb{V}_h(\Omega, \Gamma))$ , see *i*) of Lemma 5.1 and (25). So  $\mathbf{w} = \mathcal{R}(\mathbf{u})$  for some  $\mathbf{u} \in \mathbb{V}_h(\Omega, \Gamma)$ , and  $A_{\Omega \times \Gamma}(\mathbf{u}) = \mathcal{R}^*A\mathcal{R}(\mathbf{u}) = \mathcal{R}^*A\mathbf{w} = \mathcal{R}^*B^*\mathbf{p} = B^*R^*\mathbf{p} = 0$  since  $\mathbf{p} \in \mathbb{X}_h(\Sigma)^\circ = (R(\mathbb{V}_h(\Sigma)))^\circ = \text{Ker } R^*$  by (5). As a consequence,  $\mathbf{u} \in \text{Ker}(A_{\Omega \times \Gamma})$  and  $\Phi(\mathbf{u}) = \mathbf{p} - iT(\mathbf{v}) = \mathbf{q}_-$ .  $\square$

### Theorem 7.3.

Assume one of the hypotheses of Lemma 6.2. Then  $\dim \text{Ker}(A_{\Omega \times \Gamma}) = \dim(\text{Ker}(A) \cap \text{Ker}(B)) + \dim \text{Ker}(\text{Id} + \text{IIS})$ .

*Proof.* Using the rank-nullity theorem,  $\dim \text{Ker}(A_{\Omega \times \Gamma}) = \dim \text{Ker}(\Phi) + \dim \text{Im}(\Phi)$ . Then  $\dim \text{Ker}(\Phi) = \dim(\text{Ker}(A) \cap \text{Ker}(B))$  by Proposition 7.1, and  $\dim \text{Im}(\Phi) = \dim \text{Ker}(\text{Id} + \text{IIS})$  by Proposition 7.2. This concludes the proof.  $\square$

Note that Theorem 7.3 holds no matter the specific choice of the impedance operator  $T$ , as soon as it induces a scalar product, i.e. it complies with (26). Theorem 7.3 adapts [20, Propositions 8.2 and 8.4] to the discrete setting and, at the same time, provides an extension since in the present case we do not assume that  $\text{Ker}(A) \cap \text{Ker}(B) = \{0\}$ . The case  $\text{Ker}(A) \cap \text{Ker}(B) \neq \{0\}$  covers situations where FEM-BEM couplings satisfying Assumption (16) suffer from a spurious resonance phenomenon.

An interesting consequence of the formula of Theorem 7.3 is that, if  $A_{\Omega \times \Gamma}$  is invertible, then, systematically, both  $A - iB^*TB$  (see Lemma 6.2) and  $\text{Id} + \text{IIS}$  are invertible. On the other hand, if  $A - iB^*TB$  is invertible, then  $\text{Ker}(A) \cap \text{Ker}(B) = \{0\}$ , see Lemma 6.2. This occurs for example when imposing local boundary conditions such as Dirichlet, Neumann or Robin conditions on  $\Gamma$ . In that case the map  $\Phi$  establishes an isomorphism between  $\text{Ker}(A_{\Omega \times \Gamma})$  and  $\text{Ker}(\text{Id} + \text{IIS})$ . Finally, [11] establishes that  $\text{Ker}(A_\Gamma - iB_\Gamma^*T_\Gamma B_\Gamma)$  and  $\text{Ker}(A_{\Omega \times \Gamma})$  are either simultaneously trivial or non-trivial for the Costabel coupling, i.e., the dimensions are equal. Thus, we deduce from Theorem 7.3 that the substructured problem (35) is well-posed even at spurious resonances for the Costabel FEM-BEM coupling!

## 8 Inf-sup estimates

We have just seen that, under the hypothesis  $\text{Ker}(A) \cap \text{Ker}(B) = \{0\}$ , the operators  $A_{\Omega \times \Gamma}$  and  $\text{Id} + \text{IIS}$  are simultaneously both invertible or both non-invertible. Keeping the hypothesis  $\text{Ker}(A) \cap \text{Ker}(B) = \{0\}$ , we wish to discuss how the inf-sup constants of these two operators compare. For this we need to introduce a few constants. First, we define two constants related to the boundary trace operator

$$\begin{aligned} t_h^- &:= \inf_{\mathbf{p} \in \mathbb{V}_h(\Sigma)^* \setminus \{0\}} \|B^*(\mathbf{p})\|_{\mathbb{V}_h(\Omega)^*} / \|\mathbf{p}\|_{T^{-1}} \\ t_h^+ &:= \sup_{\mathbf{p} \in \mathbb{V}_h(\Sigma)^* \setminus \{0\}} \|B^*(\mathbf{p})\|_{\mathbb{V}_h(\Omega)^*} / \|\mathbf{p}\|_{T^{-1}} \end{aligned}$$

These are the extremal singular values of the operator  $B^*$ . These two constants were thoroughly discussed in [21, Section 7] and [23], where it was shown that an appropriate choice of impedance operator  $T$  leads to  $t_h^\pm$  being  $h$ -uniformly bounded from below and above. We also need to consider the continuity modulus

$$\|A\| := \sup_{\mathbf{u} \in \mathbb{V}_h(\Omega) \setminus \{0\}} \sup_{\mathbf{v} \in \mathbb{V}_h(\Omega) \setminus \{0\}} \frac{|\langle \mathbf{v}, A(\mathbf{u}) \rangle|}{\|\mathbf{v}\|_{\mathbb{V}_h(\Omega)} \|\mathbf{u}\|_{\mathbb{V}_h(\Omega)}}.$$

The next theorem compares the inf-sup constants (see definition (1)) of the undecomposed problem (23) and of the skeleton formulation (35). We do not provide the proof of this result: for  $\text{Ker}(A_{\Omega \times \Gamma}) \neq \{0\}$ , this inequality is a direct consequence of Theorem 7.3, and, for  $\text{Ker}(A_{\Omega \times \Gamma}) = \{0\}$ , the proof closely parallels the one of [21, Propositions 8.1 and 8.4].

### Theorem 8.1.

Assume  $\text{Ker}(\mathbf{A}) \cap \text{Ker}(\mathbf{B}) = \{0\}$ . Then the following estimate holds

$$\inf_{V_h(\Omega, \Gamma) \rightarrow V_h(\Omega, \Gamma)^*} (\mathbf{A}_{\Omega \times \Gamma}) \leq ((t_h^+)^2 + (2\|\mathbf{A}\|/t_h^-)^2) \inf_{V_h(\Sigma)^* \rightarrow V_h(\Sigma)^*} (\mathbf{Id} + \mathbf{PIS}).$$

Recall that both  $\Pi$  and  $\mathbf{S}$  are contractive<sup>2</sup> in the norm  $\|\cdot\|_{T^{-1}}$  (see Lemma 5.3 and Proposition 6.7), so following again the same argumentation as in [21, Corollary 6.2], the previous estimate combined with the contractivity of  $\mathbf{PIS}$  implies the strong coercivity of the skeleton operator  $\mathbf{Id} + \mathbf{PIS}$ .

### Corollary 8.2.

Consider that  $\text{Ker}(\mathbf{A}) \cap \text{Ker}(\mathbf{B}) = \{0\}$  and the imaginary sign assumption (28) holds. Then we have the estimate

$$\inf_{\mathbf{p} \in V_h(\Sigma)^* \setminus \{0\}} \frac{\Re\{\langle (\mathbf{Id} + \mathbf{PIS})\mathbf{p}, T^{-1}\bar{\mathbf{p}} \rangle\}}{\|\mathbf{p}\|_{T^{-1}}^2} \geq \frac{1}{2} \left( \frac{\alpha_h}{(t_h^+)^2 + (2\|\mathbf{A}\|/t_h^-)^2} \right)^2$$

with  $\alpha_h := \inf_{V_h(\Omega, \Gamma) \rightarrow V_h(\Omega, \Gamma)^*} (\mathbf{A}_{\Omega \times \Gamma})$ .

### Remark 8.3.

Assume that (17) admits a unique solution and no physical resonance phenomenon is occurring. The impedance operator  $T$  can be chosen appropriately so as to guarantee that the constants  $t_h^\pm$  are  $h$ -uniformly bounded from below and above, see e.g. [23]. With such a choice of impedance, since the discretization can reasonably be assumed stable, i.e.  $\liminf_{h \rightarrow 0} \alpha_h > 0$ , the inequality in Corollary 8.2 provides  $h$ -uniform coercivity estimate. Such an estimate guarantees  $h$ -robust convergence of classical linear iterative solvers such as GMRes.

On the other hand, the present analysis covers FEM-BEM coupling schemes such as (20) for which we are able to prove a convergence bound, see Theorem 10.1. To our knowledge, this yields the first  $h$ -robust iterative algorithm for FEM-BEM coupling with guaranteed convergence bounds.

## 9 Extension to more general problems

The theory developed so far can be generalized to boundary value problems that combine both Problems (11a) and (11b). In addition to  $\Omega$ , let  $\Omega_O \subset \mathbb{R}^d$  be a polyhedral open set (not necessarily bounded nor connected) with bounded boundary and  $\Omega_O \cap \Omega = \emptyset$ . The wavenumber is constant in the BEM subdomain  $\Omega_B = \mathbb{R}^d \setminus (\overline{\Omega} \cup \overline{\Omega_O})$  and can vary arbitrarily in the FEM subdomain  $\Omega$ , while  $\Omega_O$  represents for instance an impenetrable obstacle (or a cavity) with a sound-soft or sound-hard boundary. Note that this configuration can include cross-points, that is, points where the three domains  $\Omega$ ,  $\Omega_O$  and  $\Omega_B$  are adjacent, like in Figure 10. Acoustic wave propagation is then modelled by the following general boundary value problem:

$$\begin{aligned} u \in H^1_{\text{loc}}(\mathbb{R}^d \setminus \overline{\Omega_O}) \text{ and } -\Delta u - \kappa^2 u = f \text{ in } \mathbb{R}^d \setminus \overline{\Omega_O} \\ + \text{ boundary condition on } \partial\Omega_O \\ + \text{ Sommerfeld's radiation condition if } \Omega_B \neq \emptyset. \end{aligned} \tag{37}$$

Note that Equation (37) also covers both the configurations considered previously: it reduces to Problem (11a) when  $\Omega_O = \mathbb{R}^d \setminus \overline{\Omega}$ , while it becomes Problem (11b) when  $\Omega_O = \emptyset$ .

We wish to give a generalization of variational formulation (17), which we remind is the starting point of our theory. Let  $\Gamma_B = \partial\Omega_B$  and  $\Gamma_O = \partial\Omega_O$ , and define the space

$$\begin{aligned} \mathcal{X}(\Omega, \Gamma_B, \Gamma_O) := \{ (v, (\psi_B, q_B), (\psi_O, q_O)) \in & \\ H^1(\Omega) \times (H^{1/2}(\Gamma_B) \times H^{-1/2}(\Gamma_B)) \times (H^{1/2}(\Gamma_O) \times H^{-1/2}(\Gamma_O)) \mid & \\ \exists \tilde{v} \in H_{\text{loc}}^1(\mathbb{R}^d \setminus \overline{\Omega_O}) \text{ such that } \tilde{v}|_{\Omega} = v, \tilde{v}|_{\Gamma_B} = \psi_B, \tilde{v}|_{\Gamma_O, c} = \psi_O \}. & \end{aligned}$$

As an analogue to (17), it can be shown (see [10]) that Problem (37) can be reformulated as:

$$\begin{aligned} \text{Find } (u, (\phi_B, p_B), (\phi_O, p_O)) \in \mathcal{X}(\Omega, \Gamma_B, \Gamma_O) \text{ such that} \\ \langle \mathcal{A}_\Omega(u), v \rangle + \langle \mathcal{A}_{\Gamma_B}(\phi_B, p_B), (\psi_B, q_B) \rangle + \langle \mathcal{A}_{\Gamma_O}(\phi_O, p_O), (\psi_O, q_O) \rangle & \\ = \langle \ell_\Omega, v \rangle + \langle \ell_{\Gamma_O}, (\psi_O, q_O) \rangle, \quad \forall (v, (\psi_B, q_B), (\psi_O, q_O)) \in \mathcal{X}(\Omega, \Gamma_B, \Gamma_O), & \end{aligned} \quad (38)$$

where  $\mathcal{A}_{\Gamma_B}$  represents a FEM-BEM coupling (see (20), (21) or (22)),  $\mathcal{A}_\Omega, \ell_\Omega$  are defined in (13), and  $\mathcal{A}_{\Gamma_O}, \ell_{\Gamma_O}$  represent a boundary condition (see (14) or (15), together with [20, Examples 3.1–3.4]). Then, the whole theory for the domain decomposition method can be seamlessly extended by replacing, in the definition of  $\Sigma$ , in the functional spaces and in the operators defined in the previous sections, the component on  $\Gamma$  with two components on  $\Gamma_B$  and  $\Gamma_O$ .

**Remark 9.1** (Strongly and weakly imposed boundary conditions).

When the boundary condition on  $\Gamma_O$  is enforced thanks to an operator  $\mathcal{A}_{\Gamma_O}$  as above, we say that the boundary condition is weakly imposed. Alternatively, the boundary condition on  $\Gamma_O$  can be strongly imposed as in classical variational formulations, by modifying the expressions of  $\mathcal{A}_\Omega, \ell_\Omega$  in (13) and possibly the variational space  $H^1(\Omega)$ . The GOSM theory holds also in the latter case. We refer to [23] for more details, in which the theory is established for Helmholtz equation in a bounded domain with strongly imposed impedance boundary condition.

## 10 Numerical experiments

As pointed out in the last paragraph of Section 6, if Assumption (16) is satisfied, the operator  $\text{Id} + \Pi_S$  from the substructured problem (35) takes the form “identity + contraction”. We choose to apply a Richardson iterative scheme (see e.g. [37]), for which geometric convergence is guaranteed, see Theorem 10.1.

In the numerical tests, Problem (17), and hence its discretization (23), are assumed well-posed, i.e., the wavenumber  $\kappa$  is chosen such that the solution is unique. Thus, as discussed at the end of Section 7,  $A - iB^*TB$  is invertible and problem (35) is well-posed. Moreover,  $A$  and  $B$  being subdomain-wise block-diagonal matrices,  $T$  is also chosen to be subdomain-wise block-diagonal, i.e.  $T := \text{diag}(T_\Gamma, T_{\Omega_1}, \dots, T_{\Omega_J})$ . Note that if each block of  $T$  is real and defines a scalar product on the local trace space, then (26) is satisfied.

We give more details on how to solve efficiently (35) in Section 10.1, we discuss the choice of transmission operators  $T_j$  in Section 10.2, and present applications for various geometries and material configurations in Section 10.3 and Section 10.4.

### 10.1 Richardson solver and geometric convergence

**Notation** We emphasize that bold quantities, such as  $\mathbf{q}$  in Problem (35), correspond to vectors of vectors, where each subvector contains the degrees of freedom (dofs) associated with the discretization of the corresponding subdomain. We denote the subvector associated with subdomains  $\Omega_j$  with a non-bold font and subscript  $j = 1, \dots, J$ , while  $j = 0$  refers to  $\Gamma$ .

**Considered unknowns** For implementation simplicity reasons<sup>4</sup>, we solve (35) after performing the change of variable  $\tilde{\mathbf{q}} = \mathbf{T}^{-1}\mathbf{q}$ . Hence, we solve a new problem with  $\tilde{\Pi} := \mathbf{T}^{-1}\Pi\mathbf{T}$ ,  $\tilde{S} := \mathbf{T}^{-1}S\mathbf{T}$  and  $\tilde{\mathbf{b}} := -2i\tilde{\Pi}\mathbf{B}(\mathbf{A} - i\mathbf{B}^*\mathbf{B})^\dagger\boldsymbol{\ell}$ , instead of  $\Pi$ ,  $S$  and  $\mathbf{b} := -2i\Pi\mathbf{B}(\mathbf{A} - i\mathbf{B}^*\mathbf{B})^\dagger\boldsymbol{\ell}$  respectively. Note that  $\tilde{\Pi}$  and  $\tilde{S}$  have the same properties as  $\Pi$  and  $S$ . In particular,  $\text{Id} + \tilde{\Pi}\tilde{S}$  takes the form “identity + contraction”, with respect to  $\|\cdot\|_{\mathbf{T}}$ . Moreover, recalling the formulas  $\Pi = 2\mathbf{T}\mathbf{R}(\mathbf{R}^*\mathbf{T}\mathbf{R})^{-1}\mathbf{R}^* - \text{Id}$  and  $S = \text{Id} + 2i\mathbf{T}\mathbf{B}(\mathbf{A} - i\mathbf{B}^*\mathbf{B})^\dagger\mathbf{B}^*$ , we see that, when computing a matrix-vector product with  $\tilde{\Pi}$  (resp.  $\tilde{S}$ ), the same numbers of products as with  $\Pi$  (resp.  $S$ ) are done. It is also of interest, even though the right-hand side is computed only once, that one less matrix-vector product is needed to compute  $\tilde{\mathbf{b}}$  than to compute  $\mathbf{b}$ . Finally, remark that  $\tilde{\Pi} = \Pi^*$ , but  $\tilde{S}$  might be different from  $S^*$  since we do not assume that  $\mathbf{A} = \mathbf{A}^*$  (which does not hold, for instance, with  $\mathbf{A}_\Gamma$  defined as in (21) or (22)).

**Iterative scheme** To solve the modified equation resulting from (35), that is,  $(\text{Id} + \tilde{\Pi}\tilde{S})\tilde{\mathbf{q}} = \tilde{\mathbf{b}}$ , we use the Richardson iteration with relaxation parameter  $\beta \in (0, 1)$ :

$$\begin{aligned}\tilde{\mathbf{q}}^{n+1} &= \tilde{\mathbf{q}}^n + \beta \left( \tilde{\mathbf{b}} - (\text{Id} + \tilde{\Pi}\tilde{S})\tilde{\mathbf{q}}^n \right) \\ &= (1 - \beta)\tilde{\mathbf{q}}^n - \beta \tilde{\Pi}\tilde{S}\tilde{\mathbf{q}}^n + \beta \tilde{\mathbf{b}}.\end{aligned}\tag{39}$$

The detailed procedure for the resulting Generalized Optimized Schwarz Method (GOSM) is presented in Algorithm 1. The core of the Richardson iteration is at lines 13 and 18. We also introduce two numerical parameters:  $N = 30000$  the maximum number of iterations allowed, and  $\varepsilon = 10^{-6}$  the tolerance threshold for the relative residual  $\|\tilde{\mathbf{b}} - (\text{Id} + \tilde{\Pi}\tilde{S})\tilde{\mathbf{q}}^n\|_2 / \|\tilde{\mathbf{b}} - (\text{Id} + \tilde{\Pi}\tilde{S})\tilde{\mathbf{q}}^0\|_2$ , under which we consider that the algorithm has converged.

---

<sup>4</sup>It is easier to consider discrete unknowns in  $\mathbb{V}_h(\Sigma)$ , rather than in its dual  $\mathbb{V}_h(\Sigma)^*$ .

---

**Algorithm 1** GOSM with Richardson iteration

---

```

1: Choose an initial  $\tilde{\mathbf{q}}$ ,  $n = 0$ 
2: for  $j = 0$  to  $J$  do
3:   Compute and store  $(\mathbf{A}_j - i\mathbf{B}_j^* \mathbf{T}_j \mathbf{B}_j)^{-1}$  ▷ LU factorization
4:    $s_j = \tilde{\mathbf{q}}_j + 2i\mathbf{B}_j (\mathbf{A}_j - i\mathbf{B}_j^* \mathbf{T}_j \mathbf{B}_j)^{-1} \mathbf{B}_j^* \mathbf{T}_j \tilde{\mathbf{q}}_j$  ▷ Local scattering
5: end for
6:  $\mathbf{g} = \tilde{\Pi} \mathbf{s}$  ▷ Global exchange
7: for  $j = 0$  to  $J$  do
8:   Compute the residual  $r_j = \tilde{\mathbf{b}}_j - (\tilde{\mathbf{q}}_j + g_j)$ 
9:    $r_j^0 = r_j$ 
10: end for
11: while  $\|\mathbf{r}\|_2 > \varepsilon \|\mathbf{r}^0\|_2$  and  $n < N$  do ▷ Stopping criterion with 2-norm
12:   for  $j = 0$  to  $J$  do
13:      $\tilde{\mathbf{q}}_j = \tilde{\mathbf{q}}_j + \beta r_j$ 
14:      $s_j = \tilde{\mathbf{q}}_j + 2i\mathbf{B}_j (\mathbf{A}_j - i\mathbf{B}_j^* \mathbf{T}_j \mathbf{B}_j)^{-1} \mathbf{B}_j^* \mathbf{T}_j \tilde{\mathbf{q}}_j$  ▷ Local scattering
15:   end for
16:    $\mathbf{g} = \tilde{\Pi} \mathbf{s}$  ▷ Global exchange
17:   for  $j = 0$  to  $J$  do
18:      $r_j = \tilde{\mathbf{b}}_j - (\tilde{\mathbf{q}}_j + g_j)$ 
19:   end for
20:    $n = n + 1$ 
21: end while
22: return  $\tilde{\mathbf{q}}$ 

```

---

**Richardson iteration properties** The Richardson iteration (39) converges if and only if  $\rho((1 - \beta)\text{Id} - \beta \tilde{\Pi} \tilde{\mathbf{S}}) < 1$ , where  $\rho(\cdot)$  denotes the spectral radius (see e.g. [37, Section 3.5]). The spectral radius being independent of a specific norm, the stopping criterion in line 11 of Algorithm 1 is computed for the discrete 2-norm. For our numerical experiments we choose  $\beta = 1/2$ . Since  $\tilde{\Pi} \tilde{\mathbf{S}}$  is T-contractive, we derive from [37, Corollary 3.33]  $\rho((1 - \beta)\text{Id} - \beta \tilde{\Pi} \tilde{\mathbf{S}}) \leq \tau_h$ , with  $\tau_h := \sqrt{1 - \gamma_h^2/4}$  and  $\gamma_h := \inf_{\tilde{\mathbf{q}} \in \mathbb{V}_h(\Sigma)^* \setminus \{0\}} \|(\text{Id} + \tilde{\Pi} \tilde{\mathbf{S}})\tilde{\mathbf{q}}\|_T / \|\tilde{\mathbf{q}}\|_T$ . We point out that depending on which impedance operator T is chosen,  $\tau_h$  may, or may not, be independent of  $h$  (see also Remark 8.3 and Section 10.2). In particular, a  $h$ -independent upper bound for the convergence rate has been proved in [23], when T is block diagonal and each of its block  $\mathbf{T}_j$  is  $h$ -uniformly stable in the following sense:

$$\text{Assumption:} \quad t_*^- := \liminf_{h \rightarrow 0} t_h^- > 0, \quad t_*^+ := \limsup_{h \rightarrow 0} t_h^+ < +\infty. \quad (40)$$

**Theorem 10.1** ([23, Corollary 10.7]).

Assume (16), (40) and  $\alpha_h > 0$ . Let  $\tilde{\mathbf{q}}^\infty \in \mathbb{V}_h(\Sigma)$  refers to the unique solution of modified Equation (35). Then,  $\liminf_{h \rightarrow 0} \gamma_h > 0$ , and for any  $0 < \gamma_* < \liminf_{h \rightarrow 0} \gamma_h$ , there exists  $h_* > 0$  such that the iterate  $\tilde{\mathbf{q}}^n$  computed by means of (39) satisfies, with  $\tau_* := 1 - \gamma_*^2/4$ , the estimate

$$\frac{\|\tilde{\mathbf{q}}^n - \tilde{\mathbf{q}}^\infty\|}{\|\tilde{\mathbf{q}}^0 - \tilde{\mathbf{q}}^\infty\|} \leq \tau_*^{n/2} \quad \forall h \in (0, h_*), \forall n \geq 0.$$

**Global exchange** The coupling between subdomains is performed by applying the exchange operator  $\tilde{\Pi}$ , at lines 6 and 16 in Algorithm 1, that is, at initialization and then at each iteration. This process is described in detail in Algorithm 2, where  $(R_j)_{0 \leq j \leq J}$  denote the block components of the restriction operator  $R$  defined in (24). Its core is at line 4, where subdomains share data between each other. This operation is the only one that might be global — see the last paragraph of Section 5. We highlight that the involved matrix  $R^*TR$  is symmetric and positive definite, see (26). Then, line 4 can be performed with the Conjugate Gradient (CG) method — we plan to apply, in a future work, efficient preconditioners available in the literature. All the other operations of Algorithm 1 are local to a given subdomain  $j$ , so the GOSM can be implemented in parallel.

---

**Algorithm 2** Apply  $\tilde{\Pi}$  to a vector  $s$

---

```

1: for  $j = 0$  to  $J$  do
2:    $c_j = R_j^* T_j s_j$                                       $\triangleright$  Local products
3: end for
4:  $u = (R^*TR)^{-1} c$                                       $\triangleright$  Global product: Solve with CG
5: for  $j = 0$  to  $J$  do
6:    $g_j = 2R_j u_j - s_j$                                       $\triangleright$  Local products
7: end for
8: return  $g$ 

```

---

**Discretization and software** Meshes have been generated using `Gmsh` [36], version 4.13.1. We have implemented the GOSM in a (sequential) library written in C++. We use  $\mathbb{P}_1$ -Lagrange finite and boundary elements. Finite element (resp. boundary element) matrices are stored in sparse (resp. dense) format. To compute the LU factorization of the blocks  $A_j - iB_j^*T_jB_j$ , we use UMFPACK [30] (resp. LAPACK [1]) for sparse (resp. dense) matrices. In future work, we plan to parallelize our GOSM code and to use a hierarchical format for the boundary element matrices, in order to solve large-scale problems.

## 10.2 Choosing transmission operators

We now describe the three types of transmission operators used in our numerical tests for a block of  $T$  associated with a subdomain  $\omega \subset \mathbb{R}^d$ . The transmission conditions are applied on  $\Gamma_\omega := \partial\omega$ .

**Transmission operator 1: local Després operator** The first one is the *local* Després operator  $T_{D,\Gamma_\omega}$ , given by  $\langle T_{D,\Gamma_\omega}(u), v \rangle_{\Gamma_\omega} = \kappa \int_{\Gamma_\omega} uv \, ds$ , of classical impedance transmission conditions, so called because it was used in [32] for the first optimized Schwarz method for the Helmholtz equation. It defines a scalar product on the local trace space, and thus can be used to define an operator  $T$  satisfying (26) on  $\Sigma$ . But it does not satisfy Assumption (40), i.e., it is *not*  $h$ -uniformly stable (see for instance [23, Section 5]).

**Transmission operator 2: Yukawa hypersingular operator** The second one, already used for instance in [25, §3.1.2], is  $T_{Y,\Gamma_\omega} := \mathcal{W}_{i\kappa,\Gamma_\omega}$ , the hypersingular operator, defined in (19), this time taking the Green kernel of a “positive Helmholtz” operator, also known as the *Yukawa operator*, that is,  $-\Delta + \kappa^2 \text{Id}$ . By definition  $T_{Y,\Gamma_\omega}$  is *non-local*, can be used to

define a transmission operator (26) and satisfies Assumption (40), see again [23, Section 5]. Since an explicit expression of the Green kernel, available only for constant  $\kappa$ , is needed to implement such operators, in practice  $T_{Y,\Gamma_\omega}$  can only be defined for homogeneous subdomains.

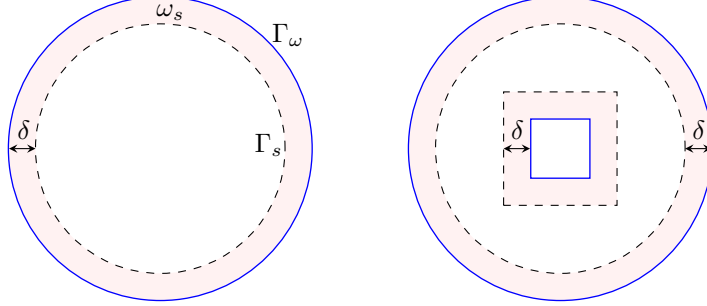


**Fig. 1** Two examples of the layer  $\omega_s \subset \omega$  to compute the Schur complement based transmission operator  $T_S$  for a subdomain  $\omega$ . The layer  $\omega_s$  is the shaded red region, and its boundary is the union of  $\Gamma_\omega := \partial\omega$  (solid blue line) and of  $\Gamma_s := \partial\omega_s \setminus \Gamma_\omega$  (dashed black line)

**Transmission operator 3: Schur complement** The last transmission operator  $T_{S,\omega}$  is a Schur complement based operator, relying on the discretization of a positive Dirichlet-to-Neumann (DtN) map for the Yukawa operator. This *non-local* operator has been first introduced in [46, Chapter 8], and then used in [26], [22, Section 4.2] and [3, Section 6]. To derive it we consider  $\omega_s \subset \omega$ , a thin layer along  $\Gamma_\omega$ , as shown in Figure 1. The boundary of  $\omega_s$  is the union of two disjoint parts, namely  $\Gamma_\omega$  and  $\Gamma_s := \partial\omega_s \setminus \Gamma_\omega$ . As in [3, Section 6], the map  $T_{S,\omega} : V_h(\Gamma_\omega) \rightarrow V_h(\Gamma_\omega)^*$  is then defined as the unique Hermitian positive definite linear map satisfying the minimization property

$$\langle T_{S,\omega}(v), \bar{v} \rangle := \min \{ \| \nabla v_s \|_{L^2(\omega_s)}^2 + \kappa^2 \| v_s \|_{L^2(\omega_s)}^2 + \kappa \| v_s \|_{L^2(\Gamma_s)}^2 \mid v_s \in V_h(\omega_s), v_s|_{\Gamma_\omega} = v \}.$$

The third term in the sum above expresses the choice of imposing homogeneous Robin boundary conditions on  $\Gamma_s$ , as in [46, Section 8.3]. The thickness  $\delta$  of the layer  $\omega_s$  is a numerical parameter, which is chosen  $h$ -independent in order for the operator to satisfy Assumption (40) (see [46, Section 8.3.3]). From now on we shall take  $\delta = \lambda/10$  as a rule of thumb, i.e. ten percent of the wavelength.

In practice, to evaluate the action  $T_{S,\omega}$ , we work with the following characterization, suitable for matrix-vector products: for  $g_D \in V_h(\Gamma_\omega)$

$$\begin{aligned} T_{S,\omega}(g_D) &= q \text{ with } (v, q) \in V_h(\omega_s) \times V_h(\Gamma_\omega)^* \text{ such that} \\ &\begin{bmatrix} A_{\omega_s} & -(B')^* \\ B' & 0 \end{bmatrix} \begin{pmatrix} v \\ q \end{pmatrix} = \begin{pmatrix} 0 \\ g_D \end{pmatrix}, \end{aligned} \tag{41}$$

where  $A_{\omega_s}$  is the matrix arising from the discretization of the Yukawa operator in  $\omega_s$ , and  $B'$  is the restriction matrix from  $\omega_s$  to  $\Gamma_\omega$ .

**Remark 10.2** (Focus on LU factorization when  $T_{S,\omega}$  is involved).

When  $T_{S,\omega}$  is chosen for the  $j$ -th subdomain, we may need to solve a local problem written as

$$(A_j - iB_j^* T_{S,\omega} B_j) u_j = B_j^* T_{S,\omega} \tilde{\alpha}_j + l_j$$

that arises from (modified) Equations (33) or (34). Since Equation (41) is more suited to compute matrix-vector products than for deriving a matrix expression, we use it to build, as in [22, §4.2], the enriched problem of the above equation:

$$\begin{bmatrix} A_j & 0 & B_j^* \\ 0 & -iA_{\omega_s} & -(B')^* \\ B_j & -B' & 0 \end{bmatrix} \begin{pmatrix} u_j \\ v \\ p \end{pmatrix} = \begin{pmatrix} l_j \\ 0 \\ i\tilde{\alpha}_j \end{pmatrix},$$

where  $p := -T_{S,\omega}(iB_j u_j + \tilde{\alpha}_j)$  is an auxiliary variable. It is on this block matrix that is applied the LU factorization of line 3 of Algorithm 1.

### 10.3 FEM-BEM coupling

From now on, we only consider Helmholtz problems in dimension  $d = 2$ . In this section, the geometry of the numerical experiments consists in a bounded domain  $\Omega$  and an unbounded homogeneous domain  $\Omega_B$  whose bounded boundary, included in  $\partial\Omega$ , is the surface denoted  $\Gamma$ , see Figures 2 and 5. Note that, for this specific geometry with  $J = 1$ ,  $\Gamma$  is also the skeleton  $\Sigma$  of the partition, and the (modified) exchange operator reads:

$$\tilde{\Pi} = \begin{bmatrix} (T_\Gamma + T_\Omega)^{-1} & 0 \\ 0 & (T_\Gamma + T_\Omega)^{-1} \end{bmatrix} \cdot \begin{bmatrix} T_\Gamma - T_\Omega & 2T_\Omega \\ 2T_\Gamma & T_\Omega - T_\Gamma \end{bmatrix}.$$

We choose  $A_\Gamma$  as one of the FEM-BEM couplings given in Section 3. Invertibility of  $A_\Gamma - iB_\Gamma^* T_\Gamma B_\Gamma$  is ensured because we have assumed that problem (17) is well-posed; so  $\kappa^2$  is not an eigenvalue of the Laplacian problem in  $\mathbb{R}^d \setminus \overline{\Omega_B}$  with homogeneous Dirichlet boundary conditions (see [11] for a proof and the expressions of the kernel of  $A_\Gamma - iB_\Gamma^* T_\Gamma B_\Gamma$  when  $\kappa$  is a spurious resonance).

#### Definition 10.3.

The simulations are run for several configurations of transmission operators, namely:

- Configuration  $D$ - $D$ , for which  $T_\Omega = T_\Gamma = T_{D,\Gamma}$ ,
- Configuration  $S$ - $S$ , for which  $T_\Omega = T_\Gamma = T_{S,\Omega}$ ,
- Configuration  $Y$ - $Y$ , for which  $T_\Omega = T_\Gamma = T_{Y,\Gamma}$ ,
- Configuration  $Y$ - $S$ , for which  $T_\Gamma = T_{Y,\Gamma}$  and  $T_\Omega = T_{S,\Omega}$ .

The configuration names refer to the subdomains, from the outside to the inside, that is, the first letter refers to the BEM subdomain, and the second one to the FEM subdomain. The thin layer needed to define  $T_{S,\Omega}$  is considered inside  $\Omega$ . The operator  $T_{Y,\Gamma}$  is defined by taking  $\Omega_B$  as the interior domain (see Section 3). Finally, note that the last three configurations only involve non-local transmission operators.

For the  $D$ - $D$ ,  $S$ - $S$  and  $Y$ - $Y$  configurations, the same transmission operator is chosen for both domains. Then,  $\tilde{\Pi}$  becomes the simple swap operator  $(p, q) \mapsto (q, p)$  and we recover the setup of classical OSMs. For the  $S$ - $S$ ,  $Y$ - $Y$  and  $Y$ - $S$  configurations, all transmission operators satisfy the  $h$ -uniform stability Assumption (40). Then, according to Definition 10.1, the convergence rate  $\tau_h$  is  $h$ -independent. This result does not hold for the  $D$ - $D$  configuration, for which an estimate similar to the one of Theorem 10.1 exists, but with  $\tau_h$  asymptotically behaving like  $1 - \mathcal{O}(h^2)(h \rightarrow 0)$ , as shown in [23, Remark 12.3]. We emphasize that the geometric convergence arises for the  $D$ - $D$  configuration because we study a discrete problem, whereas it is known that at the continuous level the convergence is not geometric, see [24].

**Matrix properties** Once discretized, classical FEM-BEM couplings (17) for the Helmholtz equation lead to block matrices where some blocks are sparse and others are dense. Mixing sparse and dense blocks can be particularly difficult to deal with for numerical solver, the choice of a software to perform an efficient LU factorization being not natural. In what follows, we highlight that depending on the choice of the transmission operators, the GOSM can also suffer from this issue, or not, when solving local problems.

*S-S* The local BEM problem  $A_\Gamma - iB_\Gamma^* T_\Gamma B_\Gamma$  mixes a sparse block and dense blocks.

*Y-Y* The local FEM problem mixes a dense block from the transmission operator and sparse blocks.

*Y-S* Transmission operators associated with each subdomain are non-local, and of the “type of their local subproblem”, *i.e.*  $A_j$  and  $T_j$  are both either sparse or dense. Thus, local problems do not mix dense and sparse blocks. Yet, transmission operators are distinct, meaning that even for a single interface the exchange operator  $\tilde{\Pi}$  is not just the swap operator, and mixes dense and sparse blocks. The difference with the previous configurations is that applying  $\tilde{\Pi}$  means solving a positive definite problem. So we can use a CG solver and only use matrix vector product of the *block diagonal* operator  $T$ , without mixing in practice dense and sparse blocks.

#### Remark 10.4.

*Avoiding mixing dense and sparse blocks also mean that in practice, one can use different optimized code for local FEM and BEM problems. For instance, one could use one-level or two-level preconditioners well-suited for FEM problems (see, e.g., [41]), while using analytic preconditioners well-suited for BEM problems (see, e.g., [2]). This is one of the motivations in using “weak”/substructured FEM-BEM couplings, see [17, 18].*

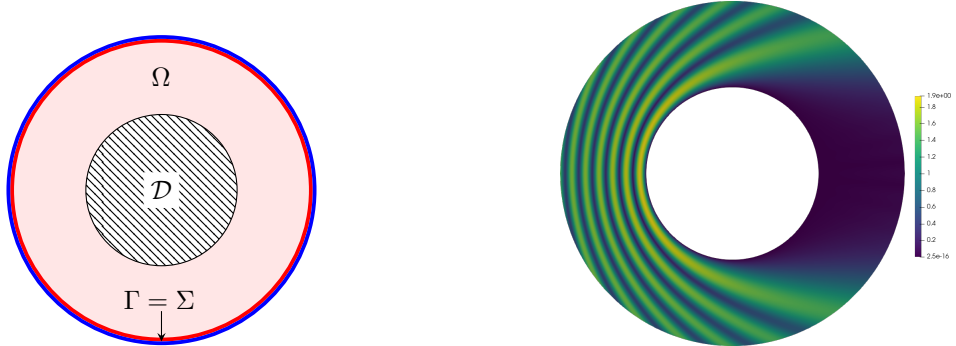
##### 10.3.1 Homogeneous problem

For the first experiment, the whole space  $\mathbb{R}^2$  is assumed homogeneous, *i.e.*  $\kappa = k > 0$  constant, except for an impenetrable disk  $\mathcal{D}$  of radius 1. We consider the problem of the scattering of an incoming plane wave  $u_i(r, \theta) = \exp(i\kappa r \cos(\theta))$ , where  $(r, \theta)$  are the polar coordinates, by the obstacle  $\mathcal{D}$ . Therefore, we solve the Dirichlet problem

$$\begin{cases} \Delta u_D + \kappa^2 u_D = 0, & \text{in } \mathbb{R}^2 \setminus \mathcal{D}, \\ u_D(r, \theta) = -u_i(r, \theta), & \text{on } \partial\mathcal{D}, \\ + \text{Sommerfeld's condition} & (12), \end{cases} \quad (42)$$

whose unique solution is  $u_D(r, \theta) := -\sum_{p \in \mathbb{Z}} i^{|p|} \exp(ip\theta) J_{|p|}(\kappa r) H_{|p|}^1(\kappa r) / H_{|p|}^1(\kappa)$ , with  $J_\nu$  the Bessel function of first kind of order  $\nu$  and  $H_\nu^1$  the Hankel function of first kind of order  $\nu$ , see e.g. [45, Chap.10].

In order for the problem to fit the framework of Problem (11b) and Equation (17), we introduce, as an artificial interface, a circle  $\Gamma$  of radius  $r = 2$ , and denote by  $\Omega$  the bounded domain whose boundary is composed of  $\Gamma$  and  $\partial\mathcal{D}$ , see Figure 2a. Even though  $\Omega$  is homogeneous, we discretize it using finite elements. In this experiment, boundary conditions on  $\partial\mathcal{D}$  are imposed strongly, that is, directly in the  $\Omega$  local problem, see Remark 9.1. In particular,



(a) Geometry considered for problem (42).  $\Sigma$  is the skeleton  
(b) Amplitude of the total field, for  $Y-S$  configuration, Costabel coupling and  $\kappa = 20$ ,  $N_\lambda = 40$

**Fig. 2** Homogeneous test case, which has an explicit expression of the exact solution

$N_\lambda$	FEM-BEM coupling	$D-D$	$Y-Y$	$S-S$	$Y-S$	$N_\lambda$	FEM-BEM coupling	$D-D$	$Y-Y$	$S-S$	$Y-S$
30	Costabel	5680	138	134	83	50	Costabel	13830	134	130	80
	Johnson-Nédélec	5857	137	132	83		Johnson-Nédélec	14946	134	134	82
	Bielak-MacCamy	5858	137	131	85		Bielak-MacCamy	14944	134	127	79
40	Costabel	9393	137	132	81	60	Costabel	18957	135	128	78
	Johnson-Nédélec	9917	136	130	86		Johnson-Nédélec	20994	133	128	80
	Bielak-MacCamy	9991	136	127	82		Bielak-MacCamy	21052	133	126	81

Table 1: Several  $N_{it}$  used to draw Figure 3 (left), for  $\kappa = 10$  and  $h\kappa = 2\pi/N_\lambda$ . See Definition 10.3 for transmission operators choices

for this geometry, and only for this geometry,  $\Gamma_\Omega = \Gamma \subsetneq \partial\Omega$ , instead of  $\partial\Omega$  as explained in Section 10.2. Thus, the transmission conditions are only set on  $\Sigma = \Gamma$ , and so is the skeleton problem (35).

**Numerical results** We denote by  $N_\lambda := (2\pi)/(\kappa h)$  the number of points per wavelength. Figure 2b shows the modulus of the total field for  $\kappa = 20$  and  $N_\lambda = 40$ . We report in Tables 1 and 2 the number of iterations  $N_{it}$  needed to reach convergence, respectively for varying  $N_\lambda$  and  $\kappa$ . For both studies, we observe that the number of iterations is roughly the same for Costabel, Johnson-Nédélec or Bielak-MacCamy couplings, even though Definition 10.1 only guarantees convergence when the first one is used. Thus, in what follows, we choose to focus on the Costabel coupling, but emphasize that all the numerical conclusions we draw are also valid for the two other FEM-BEM couplings. The number of degrees of freedom of each simulation can be found in Table 3.

### Remark 10.5.

Recovering almost the same number of iterations for the three considered FEM-BEM couplings is not a surprise. Indeed, computing explicitly, at the continuous level, the operator  $S_\Gamma$  for all three couplings leads to the common expression  $S_\Gamma = (\text{Id}/2 + \tilde{\mathcal{K}}_\Gamma + i\mathcal{T}_\Gamma\mathcal{V}_\Gamma)^{-1}(\text{Id}/2 + \tilde{\mathcal{K}}_\Gamma - i\mathcal{T}_\Gamma\mathcal{V}_\Gamma)$ . This is nothing else than the outgoing-ingoing impedance-to-impedance operator of the local BEM problem. The proof relies on Calderón identities [51, Proposition 3.6.4.]. Although, in a discretized setting, scattering operators do not coincide anymore (because Calderón identities

$\kappa$	FEM-BEM coupling	$D-D$	$Y-Y$	$S-S$	$Y-S$	$\kappa$	FEM-BEM coupling	$D-D$	$Y-Y$	$S-S$	$Y-S$
6	Costabel	4343	146	79	69	18	Costabel	10567	135	121	78
	Johnson-Nédélec	4389	147	79	68		Johnson-Nédélec	11071	135	124	79
	Bielak-MacCamy	4344	146	79	68		Bielak-MacCamy	11152	134	125	78
12	Costabel	7558	141	104	72	24	Costabel	13221	131	140	85
	Johnson-Nédélec	7959	140	102	71		Johnson-Nédélec	14107	131	144	89
	Bielak-MacCamy	7937	140	102	68		Bielak-MacCamy	14262	132	140	87

Table 2: Several  $N_{it}$  used to draw Figure 3 (right), for  $h^2\kappa^3 = (2\pi/10)^2$ . See Definition 10.3 for transmission operators choices

no more hold), this remark explains the similarities in Tables 1-2.

We begin by studying the  $h$ -dependence of each configuration of Definition 10.3 with  $\kappa = 20$  and increasing the value of  $N_\lambda$ , which consists in refining the mesh.

The evolution of the number of iterations is presented in Figure 3 (left). As expected from Theorem 10.1, the number of iteration does not grow for the configurations involving non-local operators, that is to say  $S-S$ ,  $Y-Y$  and  $Y-S$ . The curve associated with the local  $D-D$  configuration evolves asymptotically as  $\mathcal{O}(h^{1.69})$ , which is quasi-quadratic, as expected by the discussion led after Definition 10.3.

We now turn to Figure 3 (right) that reports how the number of iterations evolves when  $\kappa$  grows. To avoid numerical pollution — see [38, 39, 5, 31] —, we take  $N_\lambda = 10$  at  $\kappa = 1$ , and then refine the mesh with  $h^2\kappa^3 = (2\pi/10)^2$ . We point out that the operator  $T_{\Gamma, \Omega}$  involved in the  $S-S$  and  $Y-S$  configurations is different for each simulation, since the layer thickness  $\delta$  is inversely proportional to  $\kappa$ . The relative errors for each problem are around one percent. It appears that  $N_{it}$  grows sublinearly for  $D-D$  and  $S-S$  configurations, while it is quasi-constant for the  $Y-Y$  one. For the  $Y-S$  configuration, it seems that the behavior is a mix of those of  $S-S$  and  $Y-Y$ . Indeed, while  $\kappa \lesssim 13$  the number of iterations is quasi-constant, and once this value is reached,  $N_{it}$  grows sublinearly.

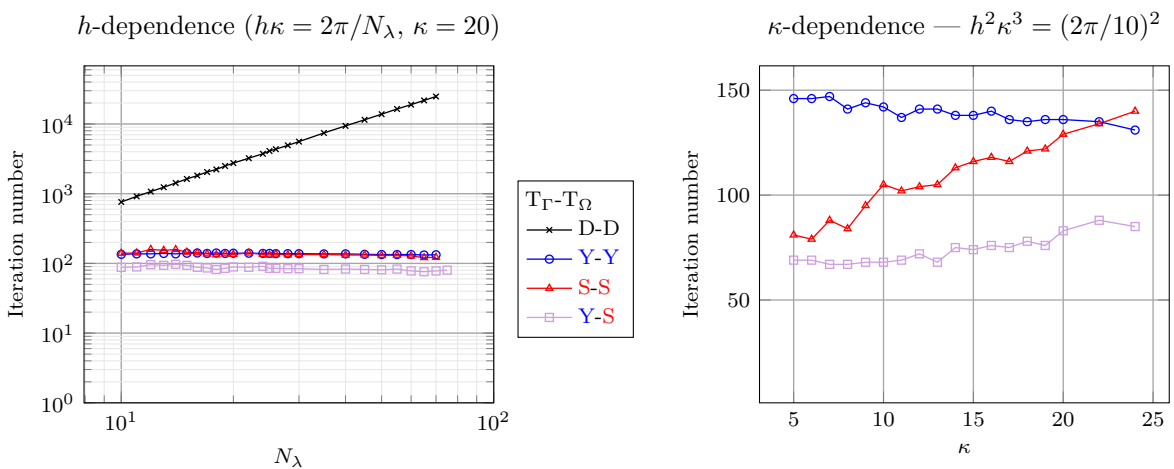


**Fig. 3** Homogeneous problem with strongly imposed Dirichlet boundary conditions and the Costabel coupling. Left,  $N_{it}$  with respect to  $N_\lambda$  for  $\kappa = 20$  and  $h\kappa = 2\pi/N_\lambda$ . Right,  $N_{it}$  with respect to the wavenumber  $\kappa$ , for  $h^2\kappa^3 = (2\pi/10)^2$

Finally, we have also led both experiences when the Dirichlet (sound-soft) boundary condition in Equation (42) is replaced by the Neumann (sound-hard) boundary condition. Then, we solve

$$\begin{cases} \Delta u_N + \kappa^2 u_N = 0, & \text{in } \mathbb{R}^2 \setminus \mathcal{D}, \\ \gamma_N(u_N)(r, \theta) = -\gamma_N(u_i)(r, \theta), & \text{on } \partial\mathcal{D}, \\ + \text{Sommerfeld's condition} & (12), \end{cases} \quad (43)$$

whose unique solution is

$$u_N(r, \theta) := - \sum_{p \in \mathbb{Z}} i^{|p|} \frac{|p| J_{|p|}(\kappa) - \kappa J_{|p|+1}(\kappa)}{|p| H_{|p|}^1(\kappa) - \kappa H_{|p|+1}^1(\kappa)} H_{|p|}^1(\kappa r) \exp(ip\theta).$$

The conclusions are the same as the ones drawn with Dirichlet boundary conditions, see Figure 4.

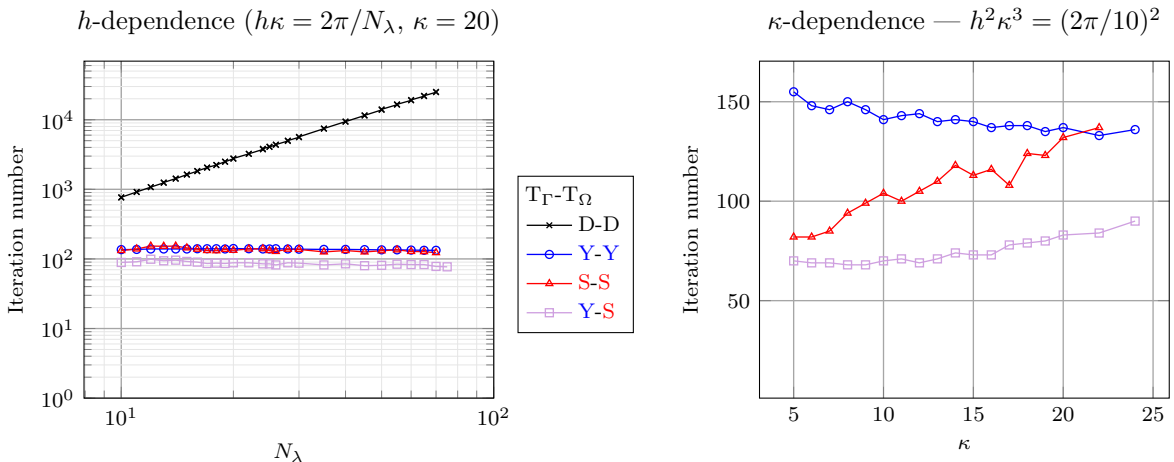


**Fig. 4** Homogeneous problem with strongly imposed Neumann boundary conditions and the Costabel coupling. Left,  $N_{it}$  with respect to  $N_\lambda$  for  $\kappa = 20$  and  $h\kappa = 2\pi/N_\lambda$ . Right,  $N_{it}$  with respect to the wavenumber  $\kappa$ , for  $h^2\kappa^3 = (2\pi/10)^2$

### 10.3.2 Heterogeneous problem

Keeping the same incident wave  $u_i(r, \theta) = \exp(ik r \cos(\theta))$ , we now consider a heterogeneous acoustic lens: the wavenumber is defined by  $\kappa(r, \theta)^2 = k^2 \eta(r, \theta)$ , with  $k > 0$  and

$$\eta(r, \theta) := \begin{cases} 1 & \text{if } r \geq 1 \\ \frac{2}{1+r^2} & \text{otherwise} \end{cases},$$

meaning that the lens is a disk of radius  $r = 1$ . We solve Problem (11b), for which the FEM subdomain  $\Omega$  is a disk of radius  $r = 2$ , whose boundary is  $\Gamma$ , and the BEM subdomain is its complement  $\mathbb{R}^d \setminus \overline{\Omega}$ , see Figure 5. Following the observations made for the previous experiment, we focus on the Costabel coupling.

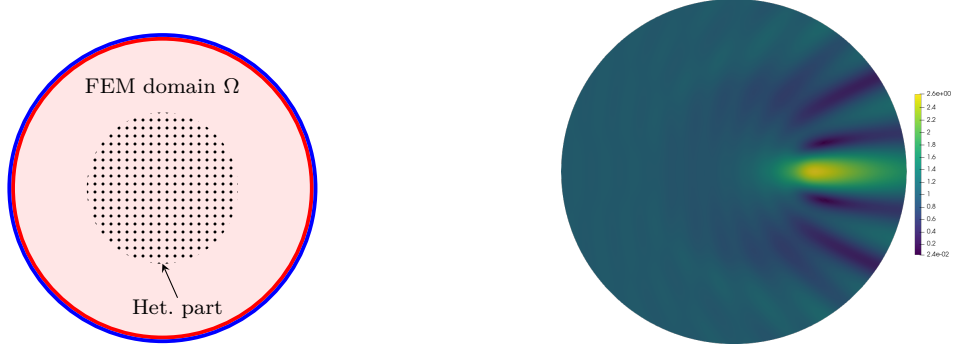


**Fig. 5** FEM subdomain  $\Omega$  with a heterogeneous pocket (left). Amplitude of the total field, for  $Y\text{-}S$  configuration, Costabel coupling and  $k = 10$ ,  $N_\lambda = 20$  (right)

Letting  $N_\lambda$  vary while taking  $k = 10$ , the results are presented in Figure 6 (left). The observations are similar to the previous experiment of Section 10.3.1, and coherent with Theorem 10.1. Indeed, the number of iterations for  $D\text{-}D$  configuration evolves asymptotically as  $\mathcal{O}(h^{1.78})$ , which is quasi-quadratic, while for the three non-local configurations  $Y\text{-}Y$ ,  $Y\text{-}S$  and  $S\text{-}S$ ,  $N_{it}$  is quasi-constant.

We now turn to Figure 6 (right), where it is shown how  $N_{it}$  evolves when  $k$  grows (numerical pollution is avoided in the same way as for the homogeneous problem). We observe asymptotically a sublinear growth for  $D\text{-}D$  and  $S\text{-}S$ , respectively  $\mathcal{O}(k^{0.86})$  and  $\mathcal{O}(k^{0.4})$ , while for  $Y\text{-}Y$  configuration,  $N_{it}$  is quasi-constant. For the  $Y\text{-}S$  configuration, the evolution of the number of iterations looks like having two states, as for the previous geometry: for  $\kappa \leq 15$  it is quasi-constant, and then it grows sublinearly. We interpret this behavior as a mix of those of  $Y\text{-}Y$  and  $S\text{-}S$  configurations. Additionally, we observe that for  $k = 15$  and 22 the number of iterations of  $S\text{-}S$  has ‘bumps’, which are also found for the  $Y\text{-}S$  configuration.

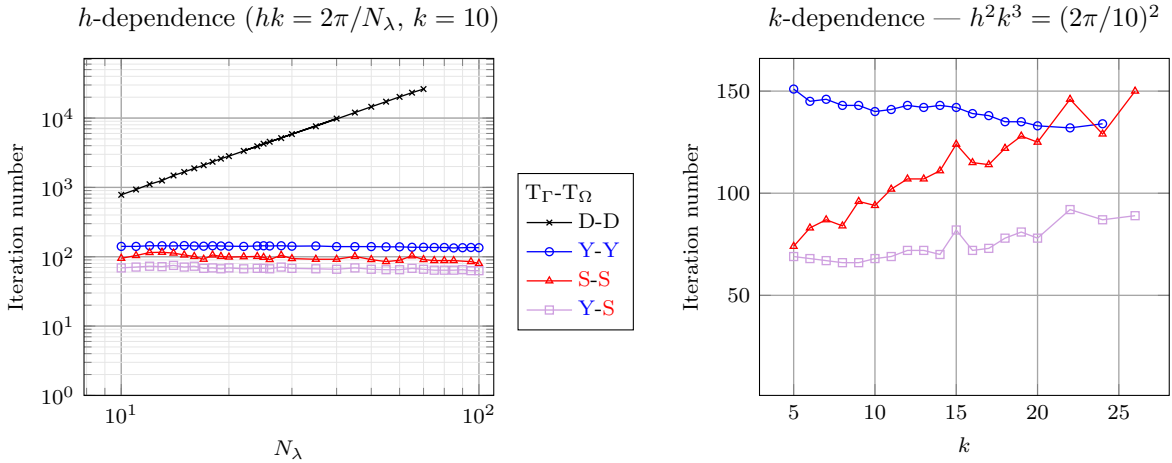


**Fig. 6** Heterogeneous problem with the Costabel coupling. Left,  $N_{it}$  with respect to  $N_\lambda$  for  $k = 10$  and  $hk = 2\pi/N_\lambda$ . Right,  $N_{it}$  with respect to  $k$  with  $h^2 k^3 = (2\pi/10)^2$ . The number of degrees of freedom of each simulation can be found in Table 4

### 10.3.3 Conclusions

Overall, for the two material settings the worst number of iterations is obtained with *D-D* configuration, whether when refining the mesh or for increasing  $\kappa$ , and the *Y-S* configuration is the one for which  $N_{it}$  is the smallest. We remind that, in the latter configuration, each transmission operator is of the same type as its respective subproblem, see the discussion in the introduction of Section 10.3.

Besides, note that configurations such as *S-S* and *Y-Y*, which involve the same transmission operator on a boundary shared by two subdomains  $\Omega_j$  and  $\Omega_k$ , can only be considered when either  $\Gamma_j \subset \Gamma_k$  or  $\Gamma_k \subset \Gamma_j$ . This property is not satisfied for partitions with cross-points, which are typically obtained with automatic graph partitioners. Hence, it is more realistic to use configurations such as the *Y-S* one, for which the transmission operator  $T_j$  associated with a domain  $\Omega_j$  is defined independently of its neighbouring domains.

## 10.4 FEM-BEM coupling and weakly imposed boundary conditions

Here, the space  $\mathbb{R}^2$  is decomposed into three domains:  $\Omega_B$  homogeneous and unbounded,  $\Omega$  bounded and possibly heterogeneous, and  $\Omega_O$  impenetrable, see Figure 7, and we solve problems of the form (37). Their reformulation (38) involves the operators  $\mathcal{A}_{\Gamma_B}$ ,  $\mathcal{A}_\Omega$  and  $\mathcal{A}_{\Gamma_O}$ , where  $\mathcal{A}_{\Gamma_B}$  is one of the FEM-BEM couplings introduced in Section 3, while  $\mathcal{A}_{\Gamma_O}$  corresponds to one of the boundary condition operators of Section 2.

The goal of this section is to study the impact of the transmission operator chosen for  $\Gamma_2$  on the number of iterations. Since the skeleton  $\Sigma$  is now composed of the union of several boundaries, we add a subscript to each transmission operator in order to indicate the transmission boundary on which it is defined. Following the conclusions drawn in Section 10.3.3, we choose  $T_B = T_{Y,\Gamma_B}$  and  $T = T_{S,\Omega}$ . The transmission operator  $T_O$  is chosen among  $T_{Y,\Gamma_O}$ ,  $T_{S,\Omega_O}$  and  $T_{D,\Gamma_O}$ . Using the same conventions as Definition 10.3, we denote the three possible configurations respectively *Y-S-Y*, *Y-S-S* and *Y-S-D*. We also consider a fourth choice named *D-D-D* for which  $T = \kappa \text{Id}$  on each boundary, mainly to compare it with *Y-S-D*. Note that  $T_{Y,\Gamma_B}$  and  $T_{Y,\Gamma_O}$  are respectively defined by considering  $\Omega_B$  and  $\Omega_O$  as *interior* domain (see Section 3), while the thin layer needed to define  $T_{S,\Omega}$  and  $T_{S,\Omega_O}$  are respectively taken inside  $\Omega$  and  $\Omega_O$ .

### 10.4.1 Homogeneous problem with weakly imposed boundary conditions

We consider the same problems (42) and (43) as in Section 10.3.1, but now the Dirichlet or Neumann boundary conditions are weakly imposed, see Remark 9.1. Thus,  $\Gamma_O$  has to be understood as a subdomain too, and is part of the skeleton  $\Sigma$ , see Figure 7. We emphasize that transmission conditions now also arise on  $\Gamma_O$ , meaning that the boundary of  $\Omega$  involved in the GOSM is larger than the one of Section 10.3.

We start by studying the Dirichlet problem for a fixed wavenumber while  $N_\lambda$  varies; results are in Figure 8 (left). As expected, when  $T_{D,\Gamma_O}$  is used for at least one domain (*Y-S-D* and *D-D-D*), we observe a quasi-quadratic growth of the number of iterations. Moreover,  $N_{it}$  is smaller with *Y-S-D* configuration, in which only  $T_{D,\Gamma_O}$  is considered, than with *D-D-D* configuration. Nonetheless, the number of iterations is greater than the configurations involving only non-local operators: for *Y-S-Y* and *Y-S-S*,  $N_{it}$  remains quasi-constant, which is coherent with Theorem 10.1. The same behaviors are observed when considering Equation (43) instead,

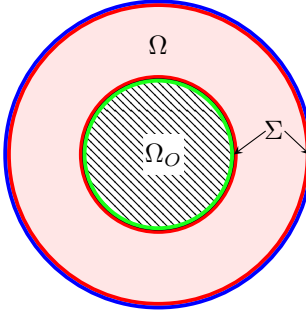


**Fig. 7** Skeleton  $\Sigma$  for FEM-BEM simulations with weakly imposed boundary conditions on  $\Gamma_2$ .  $\Gamma_B$  is the blue circle,  $\Gamma_O$  is the green circle, and  $\partial\Omega = \Sigma = \Gamma_B \cup \Gamma_O$  is the union of the two red circles

except for the  $Y\text{-}S\text{-}D$  configuration where  $N_{it}$  is also quasi-constant. One possible explanation is the following remark: the unknown  $p$  associated with  $\Gamma_O$  is theoretically equal to 0 (see [20, Example 3.2]), and numerically has converged to 0 after one iteration. This might explain why the operator chosen on  $\Gamma_O$  has an impact on the number of iterations, but not on its behavior when the mesh is refined.

Turning to the  $\kappa$ -dependence results shown in Figure 8 (right), we only study the configurations for which we have not observed any growth for  $N_{it}$  in the previous paragraph. For the Dirichlet problem,  $N_{it}$  seems quasi-constant, while for the Neumann problem, it grows sublinearly, as it was the case when considering strongly imposed boundary conditions, see Figure 4 (right). The growth is nevertheless faster. Recovering for the Neumann problem the same behavior as when the boundary condition is strongly imposed might also be due to the artificial unknown  $p$  we introduced.

#### 10.4.2 Conclusions

We conclude this study by pointing that, without considering the configurations involving the Després transmission operator,  $N_{it}$  is smaller for  $Y\text{-}S\text{-}S$  than for  $Y\text{-}S\text{-}Y$  with a Dirichlet boundary condition, while the opposite is true with a Neumann boundary condition. This indicates that the characterization of what is a good choice of transmission operator for weakly imposed boundary condition might be a matter of interest.

#### 10.4.3 Rectangular cavity problem: a configuration with cross-points

We end our numerical studies by considering in  $\mathbb{R}^2$  the scattering of a plane wave  $u_i(x, y) = \exp(i\kappa(x \cos(\theta) + y \sin(\theta)))$  by an open sound-soft rectangular cavity, with an incident angle  $\theta = 4\pi/10$ . This is modelled by Problem (37), where  $\Omega_O$  is the rectangular cavity, the FEM subdomain  $\Omega$  is the space inside the cavity,  $\Omega_B = \mathbb{R}^d \setminus (\overline{\Omega} \cup \overline{\Omega_O})$ . The wavenumber is assumed constant in  $\mathbb{R}^d \setminus \overline{\Omega_O}$ , a Dirichlet boundary condition  $u = -u_i$  is applied on  $\Gamma_O$ , and the volume source term  $f$  is null. Note that the domain decomposition involves cross-points as shown in Figure 10. This last numerical experiment aims to show the robustness to cross-points of the GOSM, even when FEM-BEM coupling is considered. More precisely, the cavity  $\Omega_O$  is an  $L_O \times l_O = 1.5 \times 0.6$  open rectangle, while  $\Omega$  is an  $L \times l = 1.3 \times 0.4$  rectangle. Note that

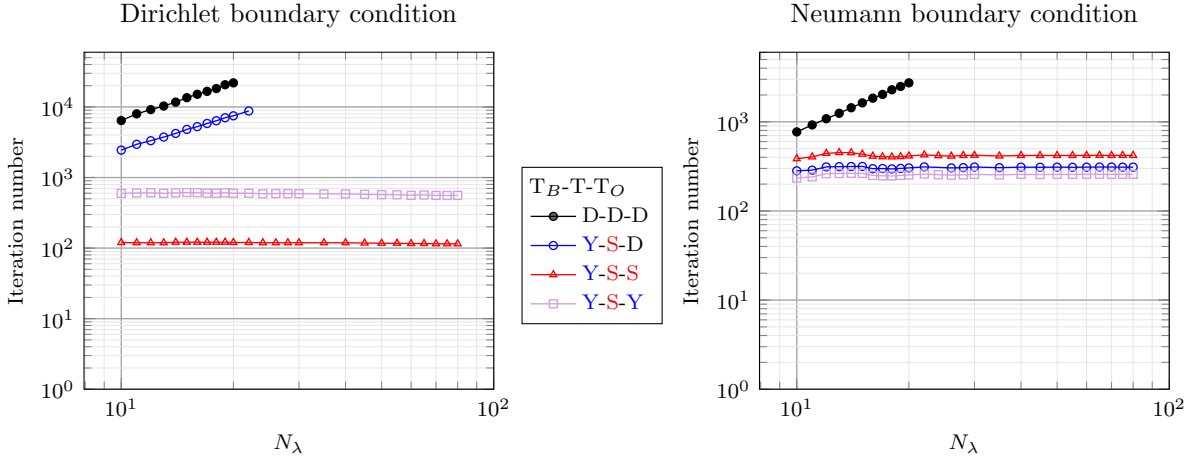


**Fig. 8**  $N_{it}$  with respect to  $N_\lambda$ . Homogeneous problem with weakly imposed boundary conditions (Dirichlet on the left and Neumann on the right), for  $\kappa = 20$ ,  $h\kappa = 2\pi/N_\lambda$ , and the Costabel coupling

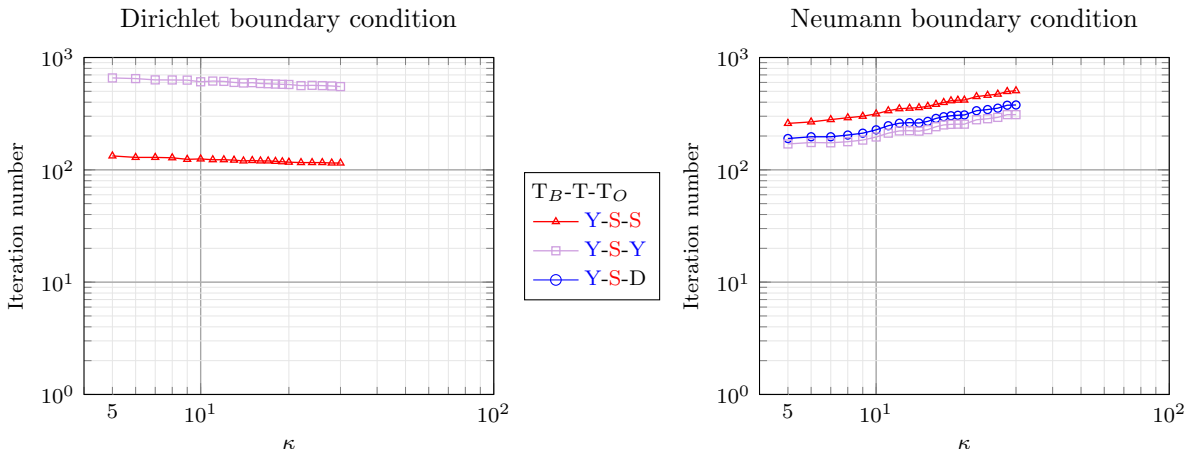


**Fig. 9**  $N_{it}$  with respect to the wavenumber  $\kappa$ . Homogeneous problem with weakly imposed boundary conditions (Dirichlet on the left and Neumann on the right), for  $h^2\kappa^3 = (2\pi/10)^2$  and the Costabel coupling

similar geometries have already been considered in [19, 33]. We also emphasize that the idea of “closing” a cavity in order to uncouple it from the rest of the space has been studied in [15] for electromagnetic wave scattering problems.

We emphasize that Problem (37) admits a unique solution for any wavenumber. Nonetheless, due to the open cavity, the problem admits *quasimodes*, i.e., functions that approximately satisfy the homogeneous problem and are spatially localized, see [33, Section 5]. For a Dirichlet boundary condition, it has been shown in [19, Section 5.6.2] that a family of quasimodes exists for  $\kappa = k_n = \pi n/l$ ,  $n \in \mathbb{N}^*$ , which are eigenvalues of the Laplacian problem with homogeneous Dirichlet boundary conditions set in  $\Omega$ . We will see that the presence of quasimodes induces an increase of the number of iterations.

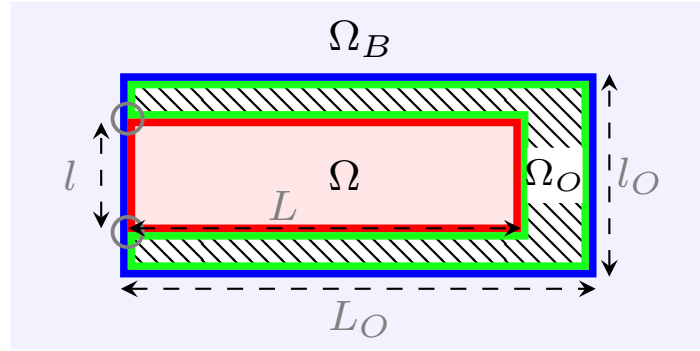


**Fig. 10** Domain decomposition for the rectangular cavity problem. Cross-points are circled in gray

The subdomains  $\Omega$  and  $\Omega_O$  being of small size, the transmission operators  $T_{S,\Omega}$  and  $T_{S,\Omega_O}$  are derived from the discretization of a positive DtN problem set in the whole domains  $\Omega$  and  $\Omega_O$  respectively, and not in a thin layer along their boundary, contrary to Section 10.2.

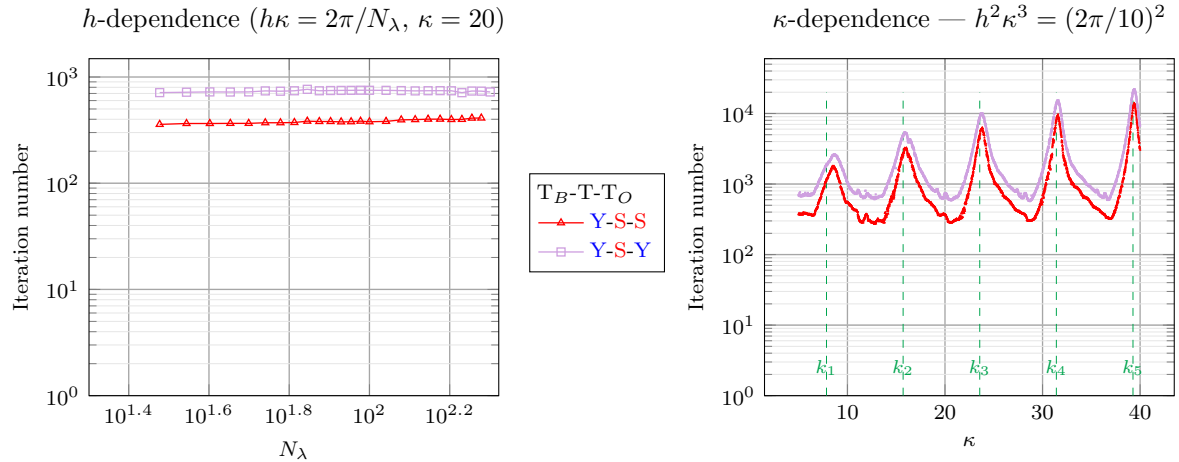


**Fig. 11** Open rectangular cavity problem with the Costabel coupling. Left,  $N_{it}$  with respect to  $N_\lambda$  for  $\kappa = 20$  and  $h\kappa = 2\pi/N_\lambda$ . Right,  $N_{it}$  with respect to  $\kappa$  with  $h^2\kappa^3 = (2\pi/10)^2$ . The dashed green lines corresponds to  $(k_n)_{n \in \mathbb{N}}$ . The number of degrees of freedom of each simulation can be found in Table 5

As in the previous sections, we start by studying the problem for a fixed wavenumber while  $N_\lambda$  varies; results are in Figure 11 (left) for  $\kappa = 20$ . In view of the observations drawn in Section 10.4.1, we only study  $Y\text{-}S\text{-}S$  and  $Y\text{-}S\text{-}Y$  configurations. We recover the same result, namely  $N_{it}$  is nearly  $h$ -independent for both configurations. Thus, the method appears to be robust to cross-points.

The behavior of the  $\kappa$ -dependence, which can be seen in Figure 11 (right), is different from the one analyzed for the homogeneous problem and its simpler geometry in Section 10.4.1. Indeed, several peaks arise around the wavenumbers  $k_n$ , represented by the vertical green dashed lines. We underline that the peaks are *not* due to some spurious resonances of BIOs,

which are the  $k_{B,nm} = \pi \sqrt{m^2/L_B^2 + n^2/l_B^2}$  for  $m, n \in \mathbb{N}^*$ . In such geometry, this phenomenon is not specific to our method, and has already been observed for FEM in [33]. Once again, when Dirichlet boundary conditions are imposed, we observe that  $N_{it}$  is smaller for  $Y\text{-}S\text{-}S$  than for  $Y\text{-}S\text{-}Y$ , as highlighted in Section 10.4.2 for a geometry without cross-points.

## A Problem sizes for the numerical experiments of Section 10.3

$N_\lambda$	$\Omega$	$\Gamma$	$N_\lambda$	$\Omega$	$\Gamma$	$\kappa$	$\Omega$	$\Gamma$	$\kappa$	$\Omega$	$\Gamma$
10	11,458	400	24	64,527	960	5	3,688	224	17	136,924	1,402
11	13,799	440	26	75,638	1,040	6	6,272	294	18	162,515	1,528
12	16,395	480	28	87,645	1,120	7	9,891	371	19	190,949	1,657
13	19,184	520	30	100,493	1,200	8	14,636	453	20	222,450	1,789
14	22,208	560	35	136,548	1,400	9	20,664	540	22	295,758	2,064
15	25,436	600	40	178,104	1,600	10	28,316	633	24	383,709	2,352
16	28,913	640	45	225,197	1,800	11	37,479	730			
17	32,576	680	50	277,787	2,000	12	48,579	832			
18	36,479	720	55	335,858	2,200	13	61,604	938			
19	40,620	760	60	399,529	2,400	14	76,798	1,048			
20	44,957	800	65	468,653	2,600	15	94,286	1,162			
22	54,308	880	70	543,254	2,800	16	114,258	1,280			

Table 3: Number of degrees of freedom in each computational domain of the homogeneous geometry, for the  $h$ -dependence (left) and  $\kappa$ -dependence (right) experiments related to Figures 3 and 4

$N_\lambda$	$\Omega$	$\Gamma$	$N_\lambda$	$\Omega$	$\Gamma$	$k$	$\Omega$	$\Gamma$	$k$	$\Omega$	$\Gamma$
10	3,814	200	30	33,499	600	5	4,774	224	20	295,364	1,789
11	4,608	220	35	45,517	700	6	8,145	294	22	392,903	2,064
12	5,458	240	40	59,379	800	7	12,904	371	24	509,959	2,352
13	6,387	260	45	75,065	900	8	19,177	453			
14	7,410	280	50	92,592	1,000	9	27,175	540			
15	8,479	300	55	111,974	1,100	10	37,270	633			
16	9,637	320	60	133,162	1,200	11	49,496	730			
17	10,875	340	65	156,221	1,300	12	64,200	832			
18	12,168	360	70	181,095	1,400	13	81,516	938			
19	13,545	380	75	207,804	1,500	14	101,663	1,048			
20	14,986	400	80	236,372	1,600	15	124,892	1,162			
22	18,115	440	85	266,755	1,700	16	151,473	1,280			
24	21,508	480	90	298,998	1,800	17	181,617	1,402			
26	25,215	520	95	333,058	1,900	18	215,631	1,528			
28	29,207	560	100	368,944	2,000	19	253,461	1,657			

Table 4: Number of degrees of freedom in each computational domain of the heterogeneous geometry, for the  $h$ -dependence (left) and  $k$ -dependence (right) experiments related to Figure 6

$N_\lambda$	$\Gamma_B$	$\Omega$	$\Gamma_O$	$N_\lambda$	$\Gamma_B$	$\Omega$	$\Gamma_O$	$\kappa$	$\Gamma_B$	$\Omega$	$\Gamma_O$	$\kappa$	$\Gamma_B$	$\Omega$	$\Gamma_O$
30	405	5,818	655	90	1,205	50,170	1,951	5.00	77	256	125	<b>23.8</b>	779	20,999	1,261
35	472	7,762	762	95	1,273	55,805	2,061	6.50	113	497	183	24.50	814	22,949	1,316
40	536	10,083	868	100	1,339	61,602	2,167	<b>8.47</b>	166	997	268	26.00	890	27,359	1,440
45	604	12,818	978	110	1,476	74,847	2,388	9.50	197	1,434	319	28.00	993	33,992	1,607
50	670	15,623	1,084	120	1,607	88,687	2,601	11.00	247	2,181	399	30.00	1,102	41,660	1,782
55	739	18,894	1,195	130	1,741	103,819	2,817	12.50	300	3,219	484	<b>31.59</b>	1,190	48,873	1,926
60	806	22,545	1,304	140	1,875	120,519	3,035	14.00	355	4,427	573	33.50	1,298	58,089	2,102
65	872	26,216	1,410	150	2,008	137,954	3,250	15.50	410	5,960	664	35.00	1,386	66,085	2,244
70	940	30,361	1,520	160	2,140	157,375	3,466	<b>16.05</b>	433	6,608	701	36.50	1,478	75,175	2,392
75	1,006	34,993	1,628	170	2,276	177,208	3,684	18.50	533	9,978	863	38.00	1,570	84,770	2,540
80	1,071	39,694	1,735	180	2,410	199,139	3,900	20.00	601	12,604	973	<b>39.39</b>	1,657	94,004	2,681
85	1,140	44,657	1,844	190	2,543	221,410	4,117	21.50	668	15,623	1,082	40.00	1,694	98,795	2,742

Table 5: Number of degrees of freedom in each computational domain of the rectangular cavity geometry, for the  $h$ -dependence (left) and  $k$ -dependence (right) experiments related to Figure 11. In bold, the wavenumbers associated with peaks tops in Figure 11

## References

- [1] E. Anderson, Z. Bai, C. Bischof, S. Blackford, J. Demmel, J. Dongarra, J. Du Croz, A. Greenbaum, S. Hammarling, A. McKenney, and D. Sorensen. *LAPACK Users' Guide*. Society for Industrial and Applied Mathematics, Philadelphia, PA, third edition, 1999.
- [2] X. Antoine and Y. Boubendir. An integral preconditioner for solving the two-dimensional scattering transmission problem using integral equations. *International Journal of Computer Mathematics*, 85(10):1473–1490, 2008.
- [3] R. Atchekzai and X. Claeys. Accelerating non-local exchange in generalized optimized Schwarz methods, 2024.
- [4] M. Aurada, M. Feischl, T. Führer, M. Karkulik, J. M. Melenk, and D. Praetorius. Classical FEM-BEM coupling methods: nonlinearities, well-posedness, and adaptivity. *Comput. Mech.*, 51(4):399–419, 2013.
- [5] I. Babuška and S. A. Sauter. Is the pollution effect of the FEM avoidable for the Helmholtz equation considering high wave numbers? *SIAM Journal on Numerical Analysis*, 34(6):2392–2423, 1997.
- [6] A. Ben-Israel and T. N. E. Greville. *Generalized inverses*, volume 15 of *CMS Books in Mathematics/Ouvrages de Mathématiques de la SMC*. Springer-Verlag, New York, second edition, 2003. Theory and applications.
- [7] A. Bendali, Y. Boubendir, and M. Fares. A FETI-like domain decomposition method for coupling finite elements and boundary elements in large-size problems of acoustic scattering. *Computers and Structures*, 85(9):526–535, may 2007.
- [8] J. Bielak and R. C. MacCamy. An exterior interface problem in two-dimensional elastodynamics. *Quart. Appl. Math.*, 41(1):143–159, 1983/84.
- [9] D. Boffi, F. Brezzi, and M. Fortin. *Mixed finite element methods and applications*, volume 44 of *Springer Ser. Comput. Math.* Berlin: Springer, 2013.
- [10] A. Boisneault, M. Bonazzoli, P. Marchand, and X. Claeys. Substructured FEM-BEM couplings together with weakly imposed boundary conditions. In preparation.

- [11] A. Boisneault, M. Bonazzoli, P. Marchand, and X. Claeys. Spurious resonances for sub-structured FEM-BEM coupling, 2025.
- [12] M. Bonazzoli and X. Claeys. Multidomain FEM-BEM coupling for acoustic scattering. *J. Integral Equations Appl.*, 36(2):129–167, 2024.
- [13] Y. Boubendir, X. Antoine, and C. Geuzaine. A quasi-optimal non-overlapping domain decomposition algorithm for the Helmholtz equation. *Journal of Computational Physics*, 231(2):262–280, 2012.
- [14] Y. Boubendir, A. Bendali, and M. B. Fares. Coupling of a non-overlapping domain decomposition method for a nodal finite element method with a boundary element method. *International Journal for Numerical Methods in Engineering*, 73(11):1624–1650, 2008.
- [15] J. Bourguignon-Mirebeau. *Préconditionnement de méthodes de décomposition de domaine pour les problèmes de diffraction d'ondes électromagnétiques impliquant une cavité profonde*. PhD thesis, Université Paris Sud - Paris XI, 2011.
- [16] H. Brezis. *Functional Analysis, Sobolev Spaces and Partial Differential Equations*. Springer New York, 2011.
- [17] B. Caudron. *Couplages FEM-BEM faibles et optimisés pour des problèmes de diffraction harmoniques en acoustique et en électromagnétisme*. PhD thesis, Université de Lorraine, Université de Liège, 2018.
- [18] B. Caudron, X. Antoine, and C. Geuzaine. Optimized weak coupling of boundary element and finite element methods for acoustic scattering. *Journal of Computational Physics*, 421:109737, 2020.
- [19] S. N. Chandler-Wilde, I. G. Graham, S. Langdon, and E. A. Spence. Numerical-asymptotic boundary integral methods in high-frequency acoustic scattering. *Acta Numerica*, 21:89–305, apr 2012.
- [20] X. Claeys. Nonlocal optimized Schwarz method for the Helmholtz equation with physical boundaries. *SIAM J. Math. Anal.*, 55(6):7490–7512, 2023.
- [21] X. Claeys. Nonselfadjoint impedance in generalized optimized Schwarz methods. *IMA J. Numer. Anal.*, 43(5):3026–3054, 2023.
- [22] X. Claeys, F. Collino, and E. Parolin. Nonlocal optimized Schwarz methods for time-harmonic electromagnetics. *Advances in Computational Mathematics*, 48(6), 2022.
- [23] X. Claeys and E. Parolin. Robust treatment of cross-points in optimized Schwarz methods. *Numer. Math.*, 151(2):405–442, 2022.
- [24] F. Collino, S. Ghanemi, and P. Joly. Domain decomposition method for harmonic wave propagation: a general presentation. *Computer Methods in Applied Mechanics and Engineering*, 184(2–4):171–211, 2000.
- [25] F. Collino, P. Joly, and M. Lecouvez. Exponentially convergent non overlapping domain decomposition methods for the Helmholtz equation. *ESAIM: Mathematical Modelling and Numerical Analysis*, 54(3):775–810, 2020.

[26] F. Collino, P. Joly, and E. Parolin. Non-local impedance operator for non-overlapping DDM for the Helmholtz equation. In *Domain Decomposition Methods in Science and Engineering XXVI*, pages 725–733. Springer International Publishing, 2022.

[27] D.L. Colton and R. Kress. *Integral equation methods in scattering theory*. Pure and Applied Mathematics (New York). John Wiley & Sons, Inc., New York, 1983.

[28] M. Costabel. Symmetric Methods for the Coupling of Finite Elements and Boundary Elements. In *Mathematical and Computational Aspects*, pages 411–420. Springer Berlin Heidelberg, 1987.

[29] M. Costabel, V. J. Ervin, and E. P. Stephan. Symmetric coupling of finite elements and boundary elements for a parabolic-elliptic interface problem. *Quart. Appl. Math.*, 48(2):265–279, 1990.

[30] T. A. Davis. Algorithm 832: UMFPACK v4.3—an unsymmetric-pattern multifrontal method. *ACM Transactions on Mathematical Software*, 30(2):196–199, 2004.

[31] A. Deraemaeker, I. Babuška, and P. Bouillard. Mesure de la dispersion pour la solution éléments finis de l'équation de Helmholtz. *Comptes Rendus de l'Académie des Sciences - Series IIB - Mechanics-Physics-Astronomy*, 327(1):103–108, 1999.

[32] B. Després. Domain decomposition method and the Helmholtz problem. *Mathematical and Numerical aspects of wave propagation phenomena*, pages 44–52, 1991.

[33] V. Dolean, P. Marchand, A. Modave, and T. Raynaud. Convergence analysis of GMRES applied to Helmholtz problems near resonances, 2025.

[34] S. Engleder and O. Steinbach. Modified boundary integral formulations for the Helmholtz equation. *Journal of Mathematical Analysis and Applications*, 331(1):396–407, jul 2007.

[35] M. J. Gander, F. Magoulès, and F. Nataf. Optimized Schwarz Methods without Overlap for the Helmholtz Equation. *SIAM Journal on Scientific Computing*, 24(1):38–60, jan 2002.

[36] C. Geuzaine and J.-F. Remacle. Gmsh: A 3-D finite element mesh generator with built-in pre- and post-processing facilities. *International Journal for Numerical Methods in Engineering*, 79(11):1309–1331, 2009.

[37] W. Hackbusch. *Iterative Solution of Large Sparse Systems of Equations*. Springer New York, 2nd edition, 2016.

[38] F. Ihlenburg. *Finite Element Analysis of Acoustic Scattering*. Springer.

[39] F. Ihlenburg and I. Babuška. Finite element solution of the Helmholtz equation with high wave number Part I: The h-version of the FEM. *Computers & Mathematics with Applications*, 30(9):9–37, 1995.

[40] C. Johnson and J.-C. Nédélec. On the coupling of boundary integral and finite element methods. *Mathematics of Computation*, 35(152):1063–1079, 1980.

[41] D. Lahaye, J. Tang, and K. Vuik. *Modern Solvers for Helmholtz Problems*. SpringerLink. Birkhäuser, Cham, 2017.

[42] W. McLean. *Strongly elliptic systems and boundary integral equations*. Cambridge University Press, Cambridge, 2000.

[43] E. H. Moore. On the reciprocal of the general algebraic matrix. *Bull. Amer. Math. Soc.*, 26:394–395, 1920.

[44] J.-C. Nédélec. *Acoustic and electromagnetic equations*, volume 144 of *Applied Mathematical Sciences*. Springer-Verlag, New York, 2001. Integral representations for harmonic problems.

[45] F. W. J. Olver, D. W. Lozier, R. F. Boisvert, and C. W. Clark, editors. *NIST handbook of mathematical functions*. U.S. Department of Commerce, National Institute of Standards and Technology, Washington, DC; Cambridge University Press, Cambridge, 2010.

[46] E. Parolin. *Non-overlapping domain decomposition methods with non-local transmission operators for harmonic wave propagation problems*. PhD thesis, Institut Polytechnique de Paris, 2020.

[47] C. Pechstein. *Finite and boundary element tearing and interconnecting solvers for multiscale problems*, volume 90 of *Lecture Notes in Computational Science and Engineering*. Springer, Heidelberg, 2013.

[48] R. Penrose. A generalized inverse for matrices. *Proc. Cambridge Philos. Soc.*, 51:406–413, 1955.

[49] W. Rudin. *Functional analysis*. New York, NY: McGraw-Hill, 2nd edition, 1991.

[50] Y. Saad. *Iterative Methods for Sparse Linear Systems*. Society for Industrial and Applied Mathematics, jan 2003.

[51] S.A. Sauter and C. Schwab. *Boundary element methods*, volume 39 of *Springer Series in Computational Mathematics*. Springer-Verlag, Berlin, 2011. Translated and expanded from the 2004 German original.

[52] F.-J. Sayas. The validity of Johnson-Nédélec’s BEM-FEM coupling on polygonal interfaces [reprint of mr2551202]. *SIAM Rev.*, 55(1):131–146, 2013.

[53] E. Schulz and R. Hiptmair. Spurious Resonances in Coupled Domain-Boundary Variational Formulations of Transmission Problems in Electromagnetism and Acoustics. *Computational Methods in Applied Mathematics*, 22(4):971–985, 2022.

[54] A. Sommerfeld. Die Greensche Funktion der Schwingungsgleichung. *Jahresbericht der Deutschen Mathematiker-Vereinigung*, 21:309–352, 1912.

[55] A. Sommerfeld. *Partial Differential Equations in Physics*. Academic Press, Inc., New York, 1949. Translated by Ernst G. Straus.

[56] O. Steinbach. A note on the stable one-equation coupling of finite and boundary elements. *SIAM J. Numer. Anal.*, 49(4):1521–1531, 2011.

[57] A. Toselli and O. Widlund. *Domain decomposition methods—algorithms and theory*, volume 34 of *Springer Series in Computational Mathematics*. Springer-Verlag, Berlin, 2005.

[58] C. H. Wilcox. Spherical means and radiation conditions. *Arch. Rational Mech. Anal.*, 3:133–148, 1959.